Electronic Supplementary Material (ESI) for Catalysis Science & Technology.

Supporting Information for:

Redox-Switchable Ring-Opening Polymerization by Tridentate ONN-Type Titanium and Zirconium Catalysts

Alicia M. Doerr, Justin M. Burroughs, Nicholas M. Legaux, and Brian K. Long*

Department of Chemistry, University of Tennessee, Knoxville, TN 37996

e-mail: long@utk.edu

Table of Contents

NMR Spectrum

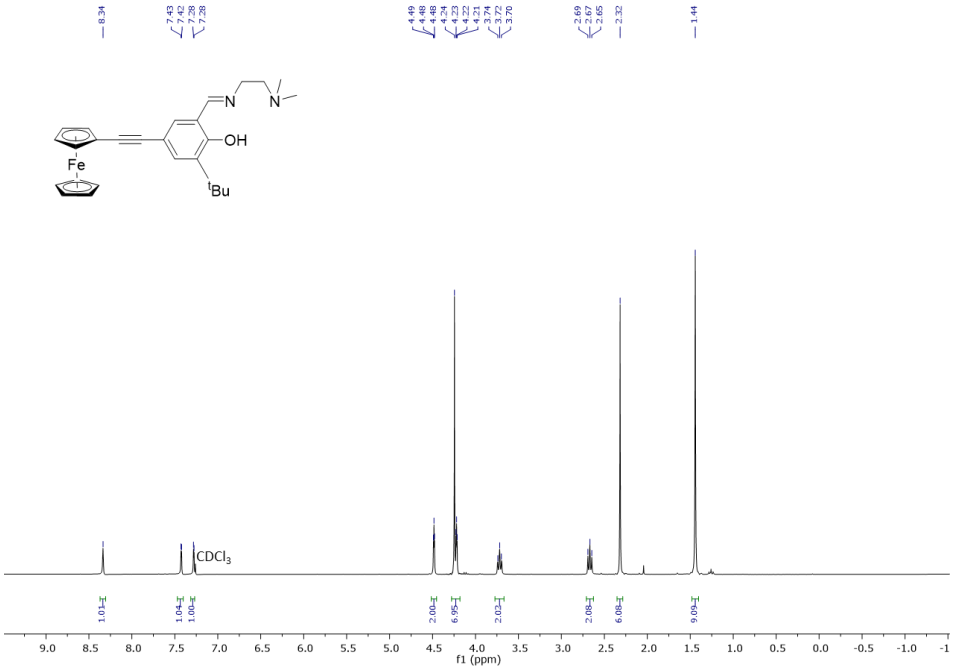

Figure S1. ^{1}H NMR (300 MHz, 25 °C, $CDCl_3$) of **L2**, δ, ppm: 1.44 (s, 9H, CH_3), 2.32 (s, 6H, NCH_3), 2.67 (t, 2H, NCH_2), 3.72 (t, 2H, NCH_2), 4.21 (t, 2H, CpH), 4.24 (s, 5H, CpH), 4.48 (t, 2H, CpH), 7.28 (d, 1H, PhH), 7.42 (d, 1H, PhH), 8.34 (s, 1H, NCH).

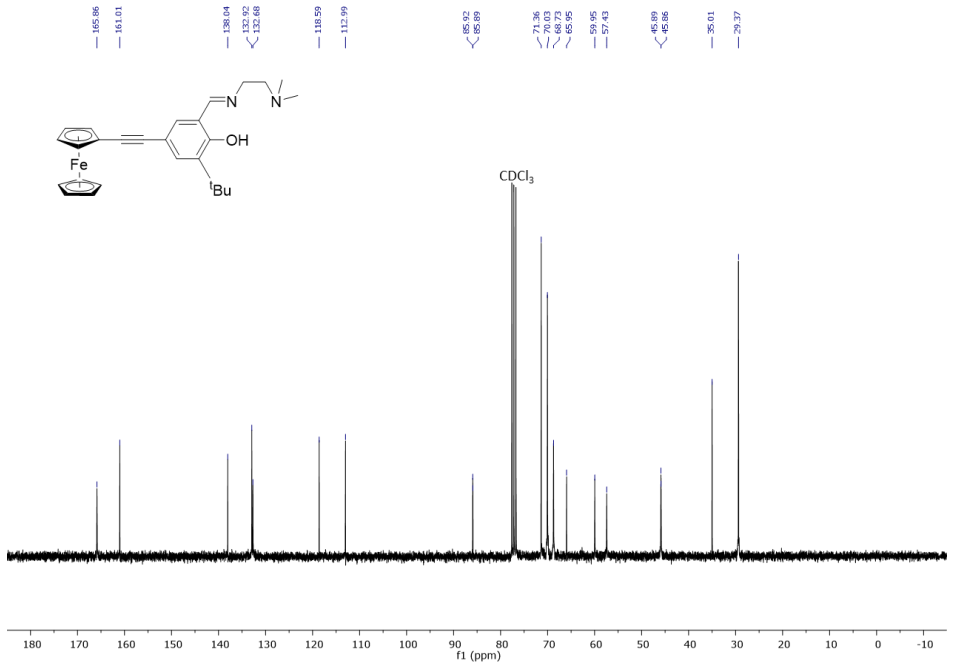

Figure S2. ^{13}C NMR (300 MHz, 25 °C, $CDCl_3$) of **L2**, δ, ppm: 29.3 (C(CH_3)), 35.0 (C(CH_3)), 45.86 (NCH_3), 45.89 (NCH_3), 57.4 (NCH_2), 59.9 (NCH_2), 65.9 (Cp-C), 68.7 (Cp-C), 70.0 (Cp-C), 71.3 (Cp-C), 85.8 (C≡C), 85.9 (C≡C), 112.9 (aromatic), 118.5 (aromatic), 132.6 (aromatic), 132.9 (aromatic), 138.0 (aromatic), 161.0 (aromatic), 165.8 (NCH).

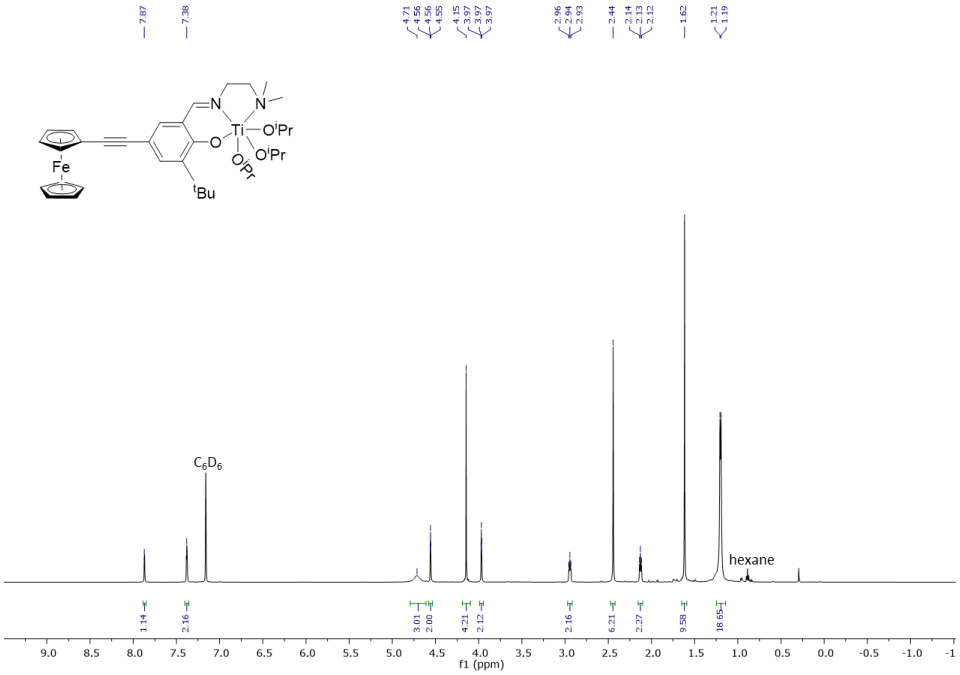

Figure S3. ^{1}H NMR (300 MHz, 25 °C, C_6D_6) of **2_{Ti}**, δ, ppm: 1.20 (d, 18H, CH_3), 1.62 (s, 9H, CH_3), 2.13 (t, 2H, NCH_2), 2.44 (s, 6H,NCH_3), 2.94 (t, 2H, NCH_2), 3.97 (t, 2H, CpH), 4.15 (s, 5H, CpH), 4.56 (t, 2H, CpH), 4.71 (br, 3H, OCH), 7.38 (s, 2H, PhH), 7.87 (s, 1H, NCH).

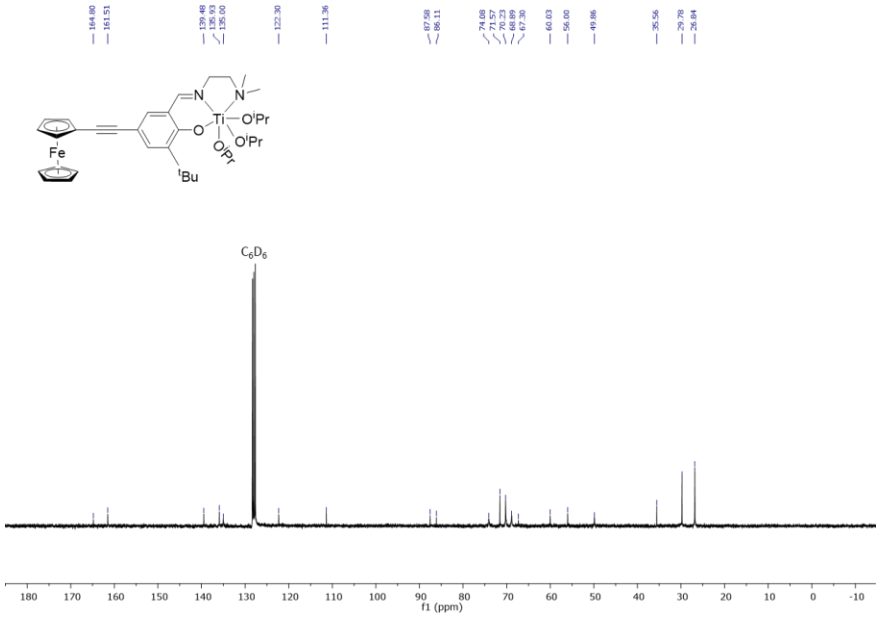

Figure S4. ^{13}C NMR (300 MHz, 25 °C, C_6D_6) of **2_{Ti}**, δ, ppm: 26.8 ($CH(CH_3)_2$), 29.7 ($C(CH_3)_3$), 35.5 ($C(CH_3)_3$), 49.8 (NCH_3), 56.0 (NCH_2), 60.0 (NCH_2), 67.3 (Cp-C), 68.8 (Cp-C), 70.2 (Cp-C), 71.5 (Cp-C), 74.0 ($CH(CH_3)_2$, 86.1 (C≡C), 87.5 (C≡C), 111.3 (aromatic), 122.3 (aromatic), 135.0 (aromatic), 135.9 (aromatic), 139.4 (aromatic), 161.5 (aromatic), 164.8 (NCH).

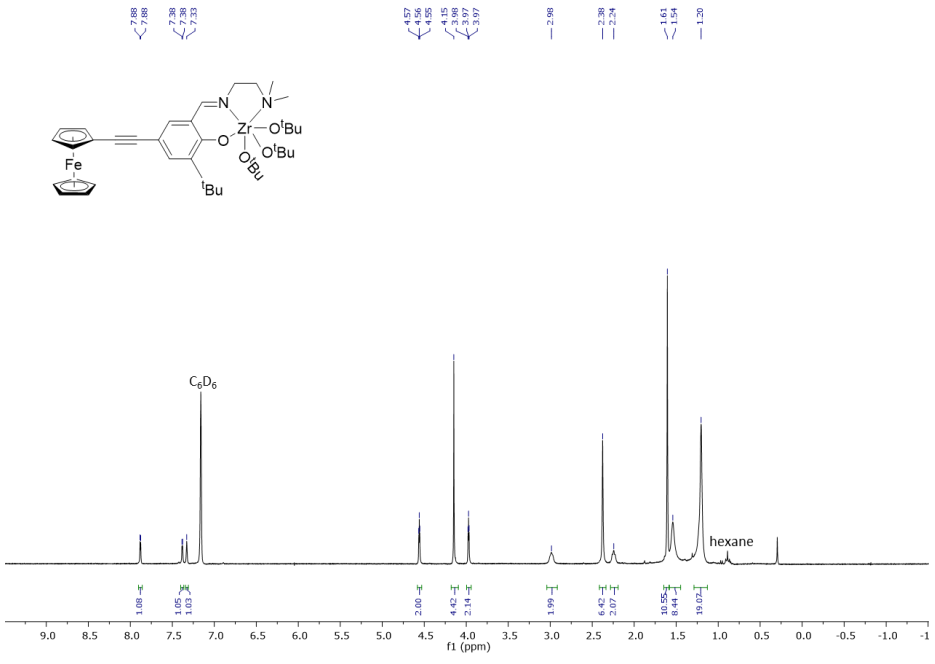

Figure S5. ^{1}H NMR (300 MHz, 25 °C, C_6D_6) of $\mathbf{2_{Zr}}$, δ, ppm: 1.20 (s, 18H, CH_3), 1.54 (s, 9H, CH_3), 1.61 (s, 9H, CH_3), 2.24 (t, 2H, NCH_2), 2.38 (s, 6H, NCH_3), 2.98 (t, 2H, NCH_2), 3.97 (t, 2H, CpH), 4.15 (s, 5H, CpH), 4.56 (t, 2H, CpH), 7.33 (s, 1H, PhH), 7.38 (d, 1H, PhH), 7.88 (d, 1H, NCH).

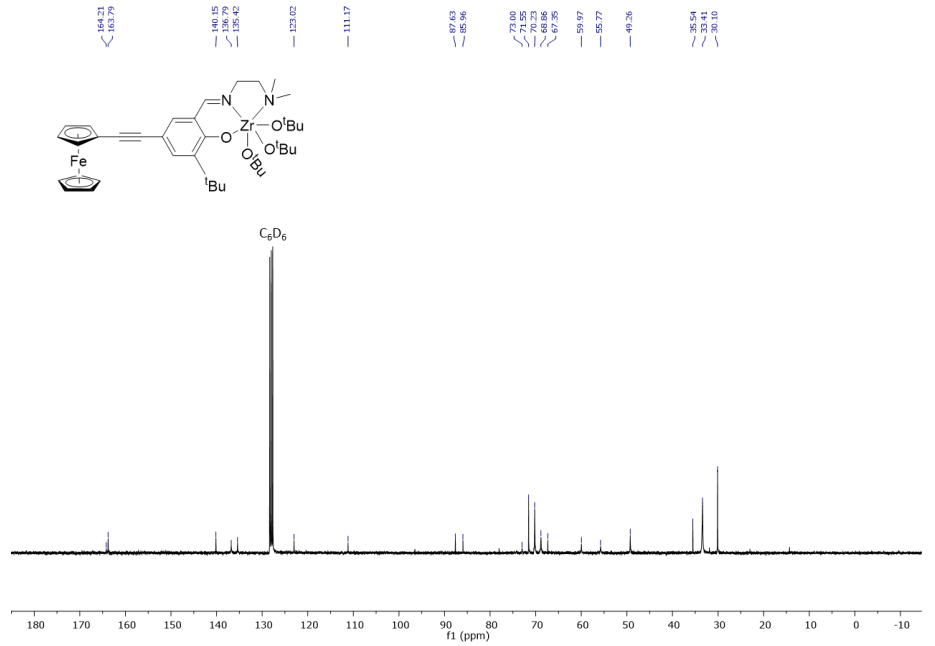

Figure S6. ^{13}C NMR (300 MHz, 25 °C, C_6D_6) of $\mathbf{2_{Zr}}$, δ, ppm: 30.1 (OC(CH_3)$_3$), 33.4 (C(CH_3)$_3$), 35.5 (C(CH$_3$)$_3$), 49.2 (NCH_3), 55.7 (NCH_2), 59.9 (NCH_2), 67.3 (Cp-C), 68.8 (Cp-C), 70.2 (Cp-C), 71.5 (Cp-C), 73.0 (OC(CH$_3$)$_3$), 85.9 (C≡C), 87.6 (C≡C), 111.1 (aromatic), 123.0 (aromatic), 135.4 (aromatic), 136.7 (aromatic), 140.1 (aromatic), 163.7 (aromatic), 164.2 (NCH).

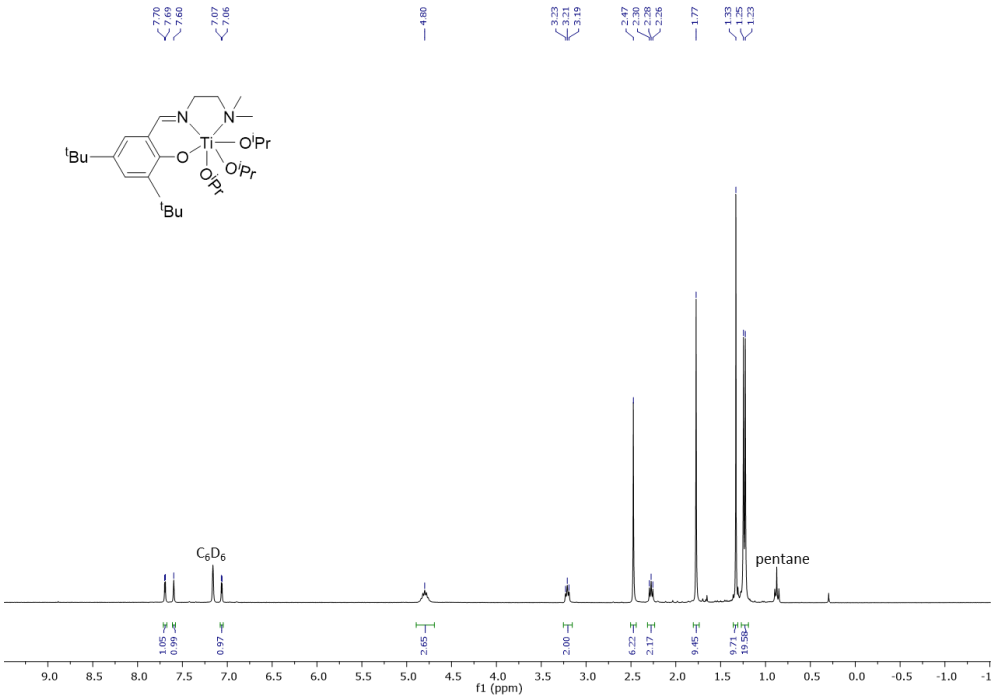

Figure S7. ^{1}H NMR (300 MHz, 25 °C, C_6D_6) of $\mathbf{3_{Ti}}$, δ, ppm: 1.23 (d, 18H, CH_3), 1.33 (s, 9H, CH_3), 1.77 (s, 9H, CH_3), 2.28 (t, 2H, NCH_2), 2.47 (s, 6H, CH_3), 3.21 (t, 2H, NCH_2), 4.80 (m, 3H, CH), 7.06 (d, 1H, PhH), 7.60 (s, 1H, NCH), 7.70 (d, 1H, PhH).

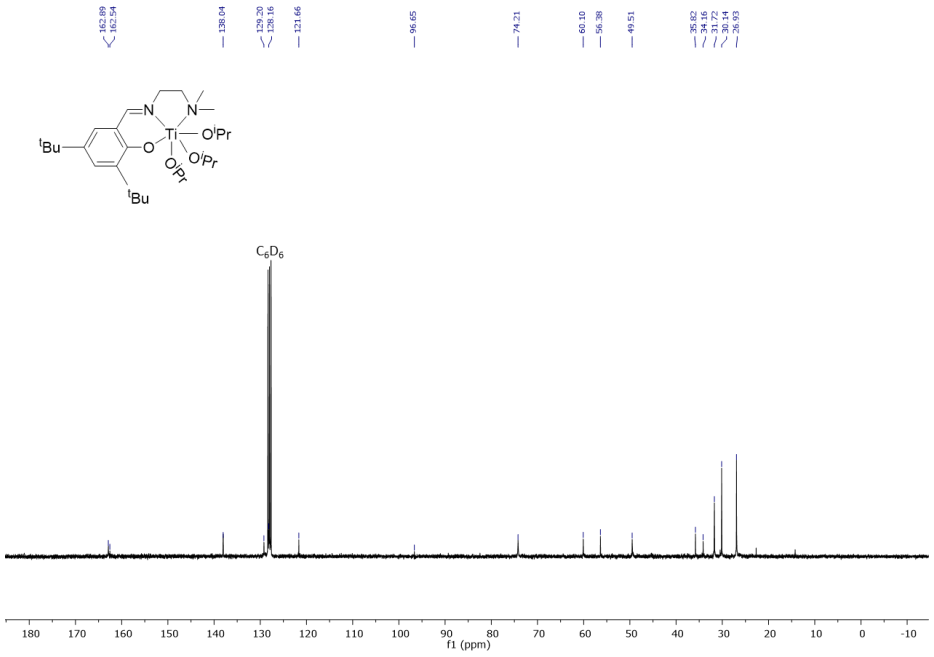

Figure S8. ^{13}C NMR (300 MHz, 25 °C, C_6D_6) of $\mathbf{3_{Ti}}$, δ, ppm: 26.9 (OCH(*C*H_3)$_2$), 30.1 (C(*C*H_3)$_3$), 31.7 (C(*C*H_3)$_3$), 34.1 (*C*(CH$_3$)$_3$), 35.8 (*C*(CH$_3$)$_3$), 49.5 (N*C*H$_3$), 56.3 (N*C*H$_2$), 60.1 (N*C*H$_2$), 74.2 (*C*(CH$_3$)$_2$), 96.6 (aromatic), 121.6 (aromatic), 128.1 (aromatic), 129.2 (aromatic), 138.0 (aromatic), 162.5 (aromatic), 162.8 (N*C*H).

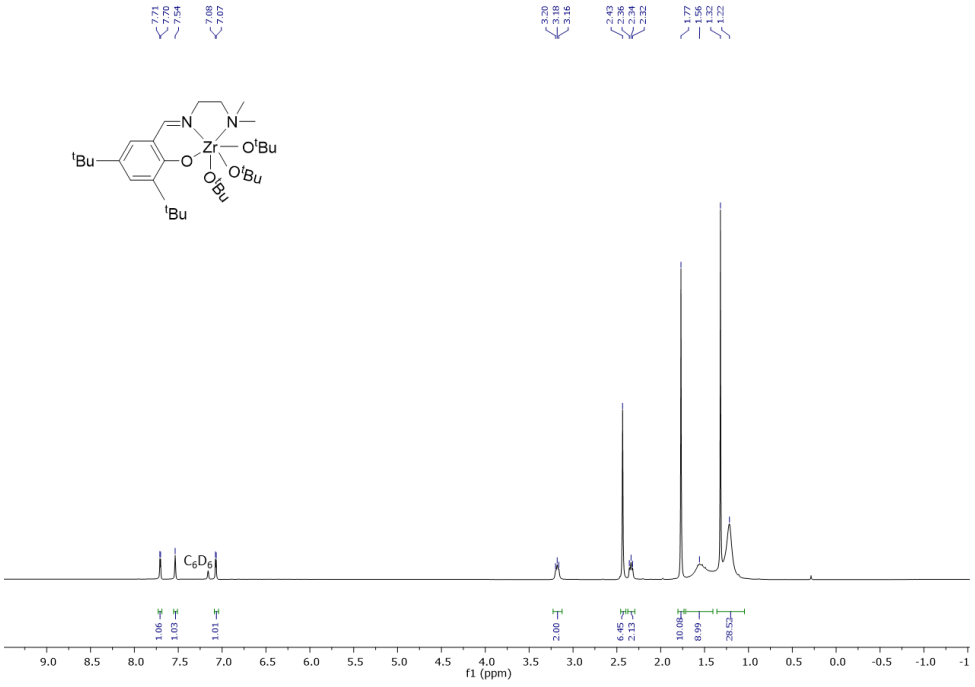

Figure S9. ^{1}H NMR (300 MHz, 25 °C, C_6D_6) of $\mathbf{3_{Zr}}$, δ, ppm: 1.22 (br, 18H, $OC(CH_3)_3$), 1.32 (s, 9H, $C(CH_3)_3$), 1.56 (br, 9H, $OC(CH_3)_3$), 1.77 (s, 9H, $C(CH_3)_3$), 2.34 (t, 2H, NCH_2), 2.43 (s, 6H, NCH_3), 3.18 (t, 2H, NCH_2), 7.08 (d, 1H, PhH), 7.54 (s, 1H, NCH), 7.71 (d, 1H, PhH).

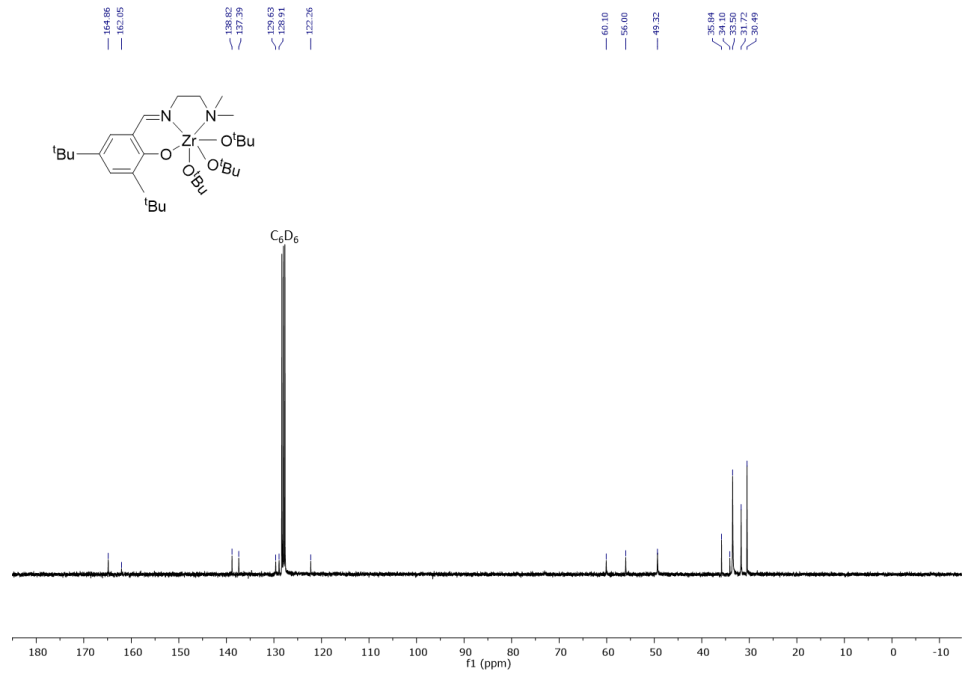

Figure S10. ^{13}C NMR (300 MHz, 25 °C, C_6D_6) of $\mathbf{3_{Zr}}$, δ, ppm: 30.4 ($OC(\mathit{C}H_3)_3$), 31.7 ($C(\mathit{C}H_3)_3$), 33.5 ($C(\mathit{C}H_3)_3$), 34.1 ($\mathit{C}(CH_3)_3$), 35.8 ($\mathit{C}(CH_3)_3$), 49.3 (NCH_3), 56.0 (NCH_2), 60.1 (NCH_2), 122.2 (aromatic), 128.9 (aromatic), 129.6 (aromatic), 137.3 (aromatic), 138.8 (aromatic), 162.0 (aromatic), 164.8 (NCH).

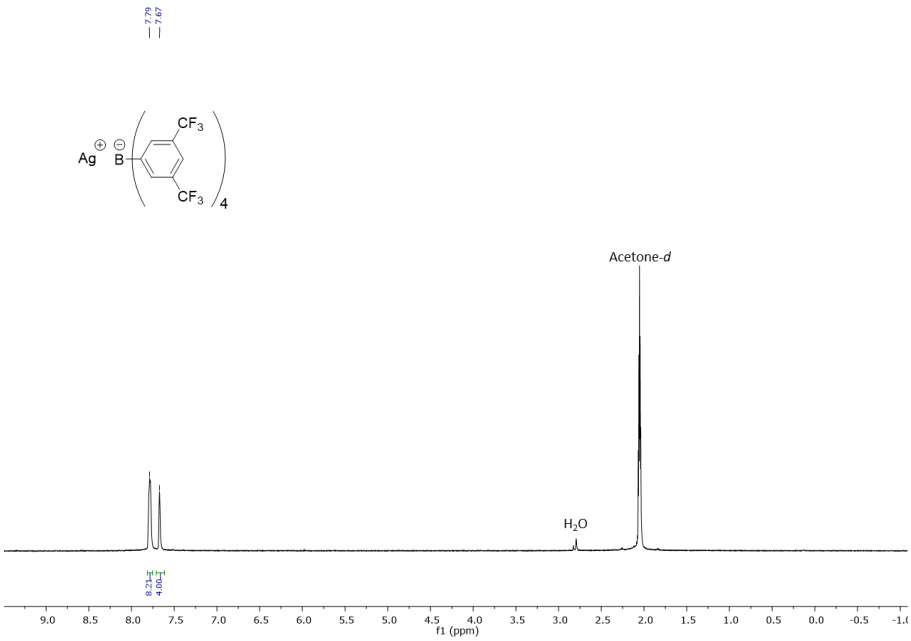

Figure 11. ^{1}H NMR (300 MHz, 25 °C, acetone-d_6) of AgBAr^{F}, δ, ppm: 7.67 (s, 4H, aromatic), 7.79 (s, 8H, aromatic).

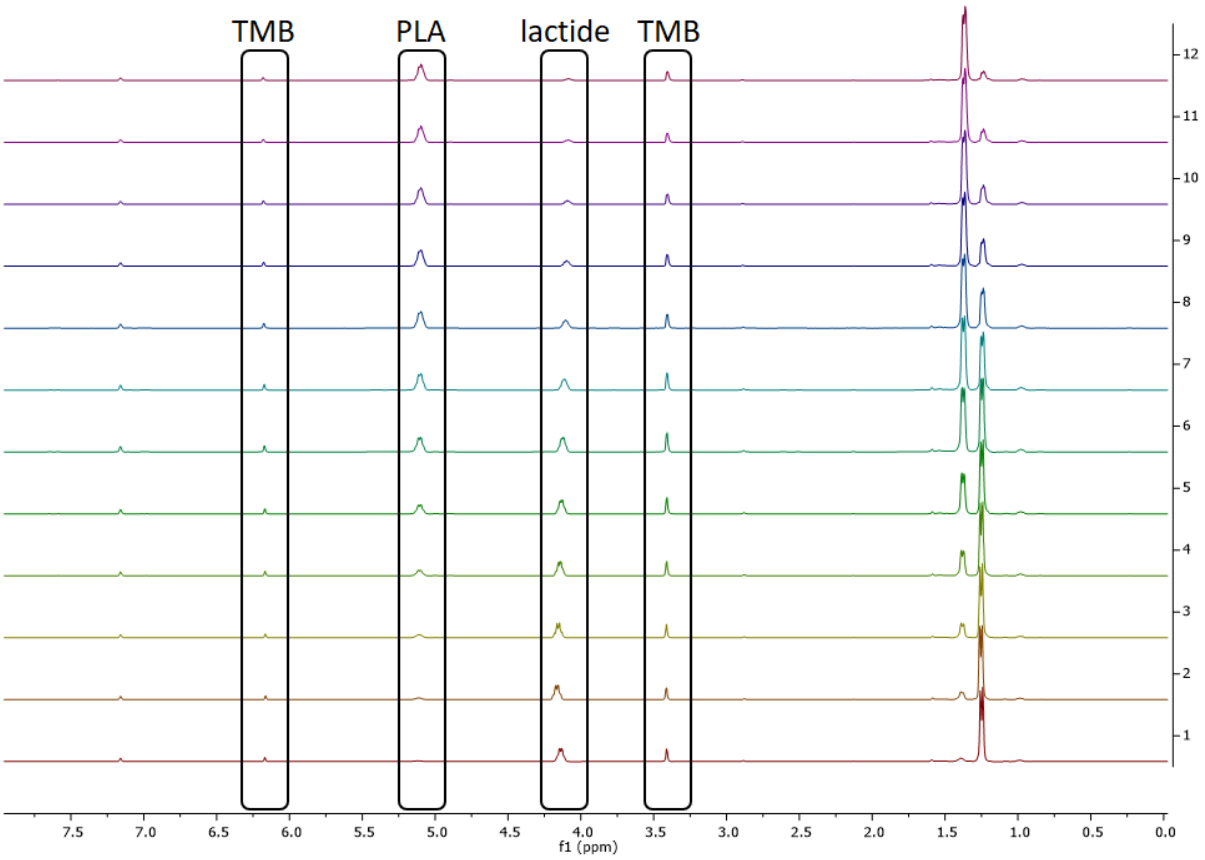

Figure S12. ^{1}H NMR spectra (400 MHz, 90 °C, C_6D_6) monitoring the polymerization of L-lactide initiated by catalyst $\mathbf{3}_{Ti}$. Each trace represents an hourly progression of the reaction starting at 1 h and ending at 12 h. The bottom trace (1 h) shows a large presence of L-lactide with little to no polymer. The top trace (12 h) shows L-lactide has been mostly converted to polylactide (PLA). Throughout the 12 h the amount of internal standard (trimethoxybenzene (TMB)) remained constant.

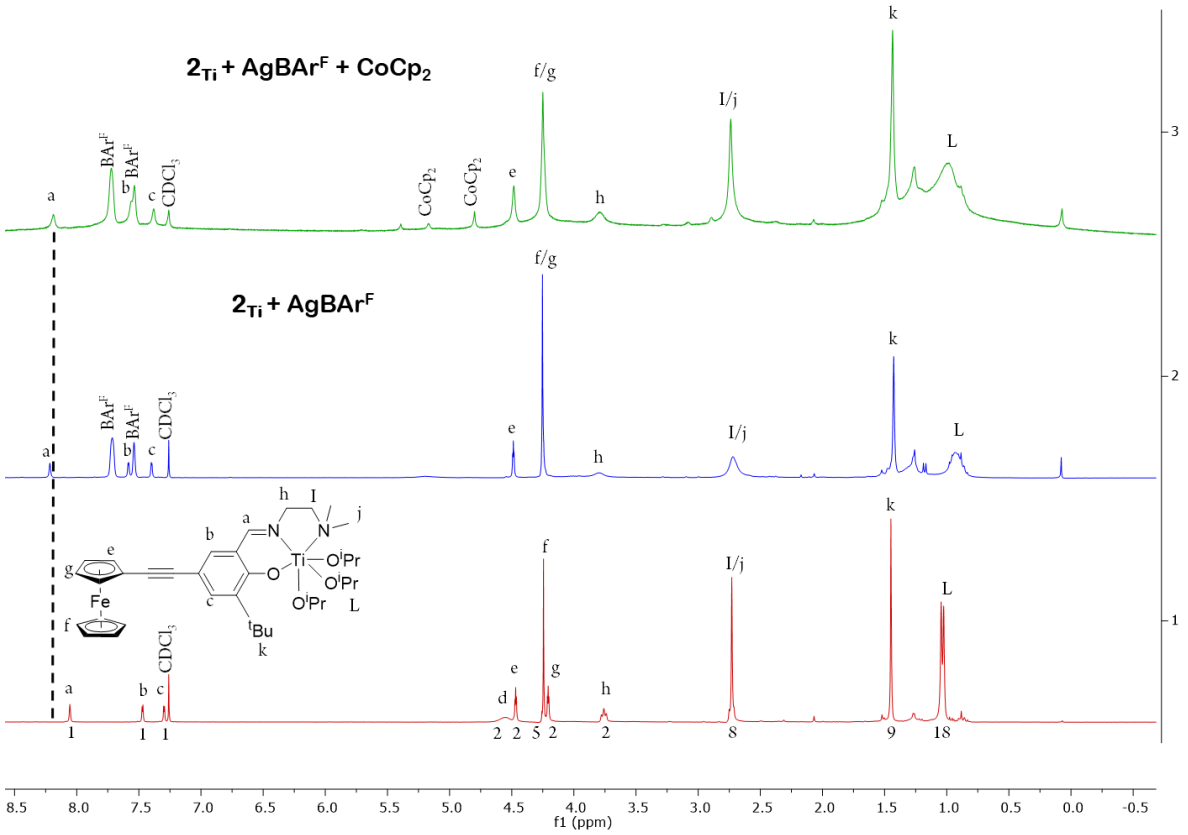

Figure S13. ^{1}H NMR spectra (300 MHz, 25 °C, $CDCl_3$) of $\mathbf{2_{Ti}}$ (bottom), $\mathbf{2_{Ti\text{-}ox}}$ (middle), and $\mathbf{2_{Ti\text{-}red}}$ (top). $\mathbf{2_{Ti\text{-}ox}}$ was generated by the addition of $AgBAr^F$ to $\mathbf{2_{Ti}}$ in $CDCl_3$ followed by filtration into a J. Young NMR tube. $\mathbf{2_{Ti\text{-}red}}$ was generated by the subsequent addition of $CoCp_2$ to the NMR tube. A shift in the peaks is seen between the bottom and middle spectra. Another shift in the peaks is seen between the middle and top spectra but the peaks in the top spectrum do not shift back to the same position as the peaks in the bottom spectrum.

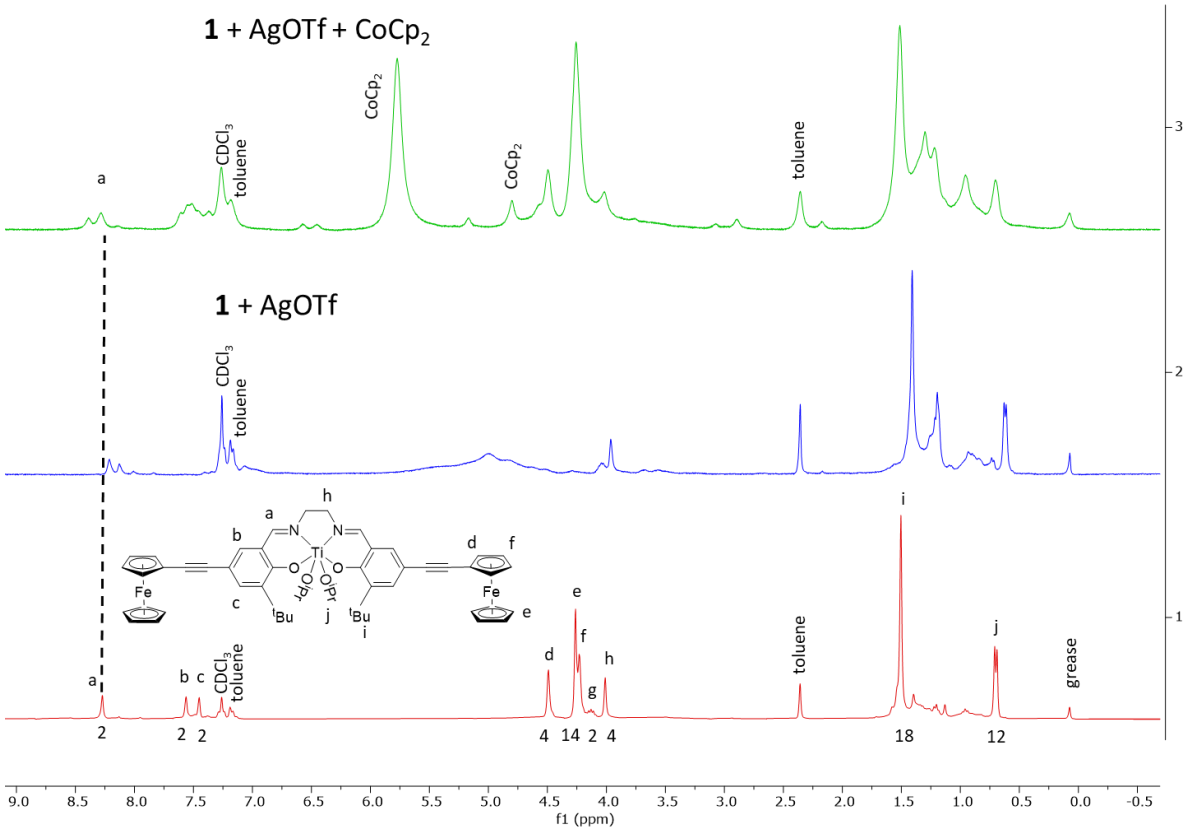

Figure S14. ^{1}H NMR spectra (300 MHz, 25 °C, $CDCl_3$) of **1** (bottom), $\mathbf{1_{ox}}$ (middle), and $\mathbf{1_{red}}$ (top). $\mathbf{1_{ox}}$ was generated by the addition of 2 equivalence of AgOTf to **1** in $CDCl_3$ in a J. Young NMR tube. $\mathbf{1_{red}}$ was generated by the subsequent addition of $CoCp_2$ to the NMR tube. A shift in the peaks is seen between the bottom and middle spectra. Another shift in the peaks is seen between the middle and top spectra but the peaks in the top spectrum do not shift back to the same position as the peaks in the bottom spectrum.

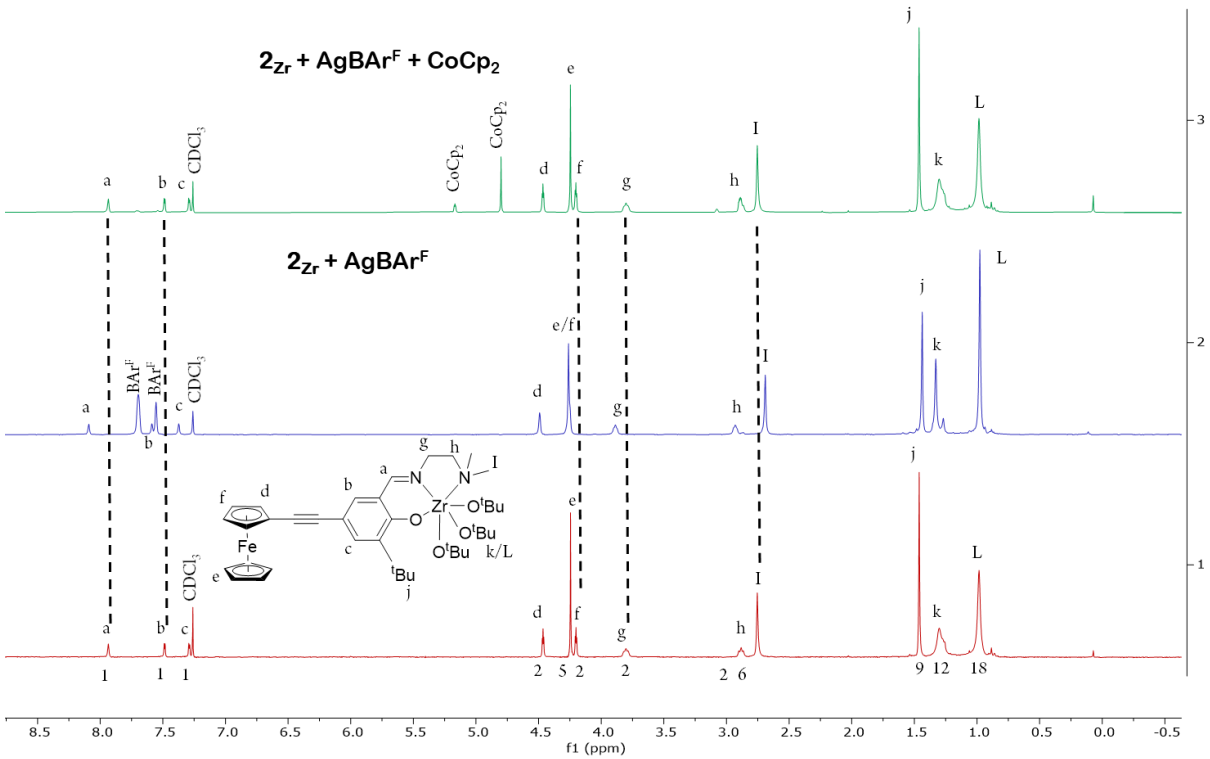

Figure S15. ^{1}H NMR spectra (300 MHz, 25 °C, $CDCl_3$) of $\mathbf{2_{Zr}}$ (bottom), $\mathbf{2_{Zr\text{-}ox}}$ (middle), and $\mathbf{2_{Zr\text{-}red}}$ (top). $\mathbf{2_{Zr\text{-}ox}}$ was generated by the addition of $AgBAr^F$ to $\mathbf{2_{Zr}}$ in $CDCl_3$ followed by heating at 90 °C for 1 h in a J. Young NMR tube. $\mathbf{2_{Zr\text{-}red}}$ was generated by the addition of $AgBAr^F$ to $\mathbf{2_{Zr}}$ in $CDCl_3$ followed by filtration into a new vial with $CoCp_2$ then addition to the NMR tube. A shift in the peaks is seen between the bottom and middle spectra. Another shift in the peaks is seen between the middle and top spectra with the peaks in the top spectrum shifting back to the same position as the peaks in the bottom spectrum.

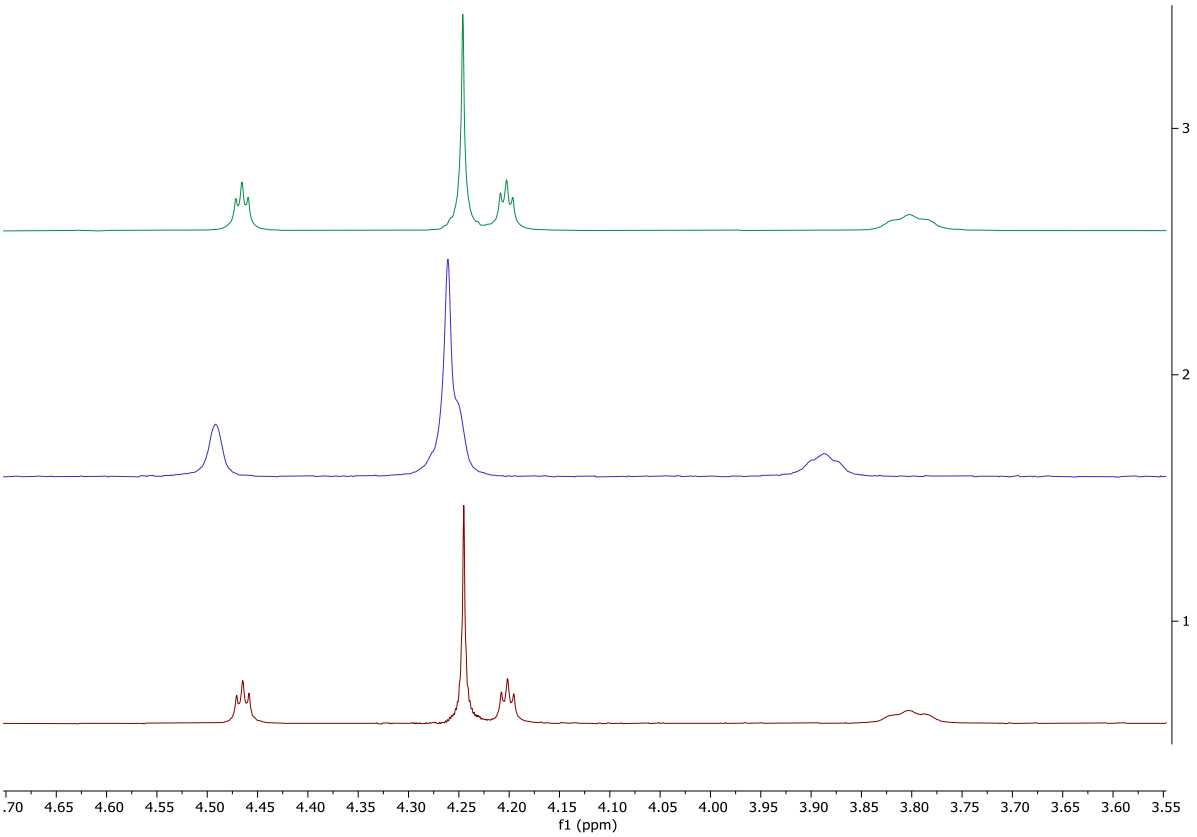

Figure S16. Zoomed in ^{1}H NMR spectra (300 MHz, 25 °C, $CDCl_3$) of $\mathbf{2_{Zr}}$ (bottom), $\mathbf{2_{Zr\text{-}ox}}$ (middle), and $\mathbf{2_{Zr\text{-}red}}$ (top). $\mathbf{2_{Zr\text{-}ox}}$ was generated by the addition of $AgBAr^F$ to $\mathbf{2_{Zr}}$ in $CDCl_3$ followed heating at 90 °C for 1 h in a J. Young NMR tube. $\mathbf{2_{Zr\text{-}red}}$ was generated by the addition of $AgBAr^F$ to $\mathbf{2_{Zr}}$ in $CDCl_3$ followed by filtration into a new vial with $CoCp_2$ then addition to the NMR tube. A broadening as well as a shift in the ferrocenyl peaks is seen between the bottom and middle spectra. Another shift in the peaks is seen between the middle and top spectra with the peaks in the top spectrum shifting back to the same position as the peaks in the bottom spectrum.

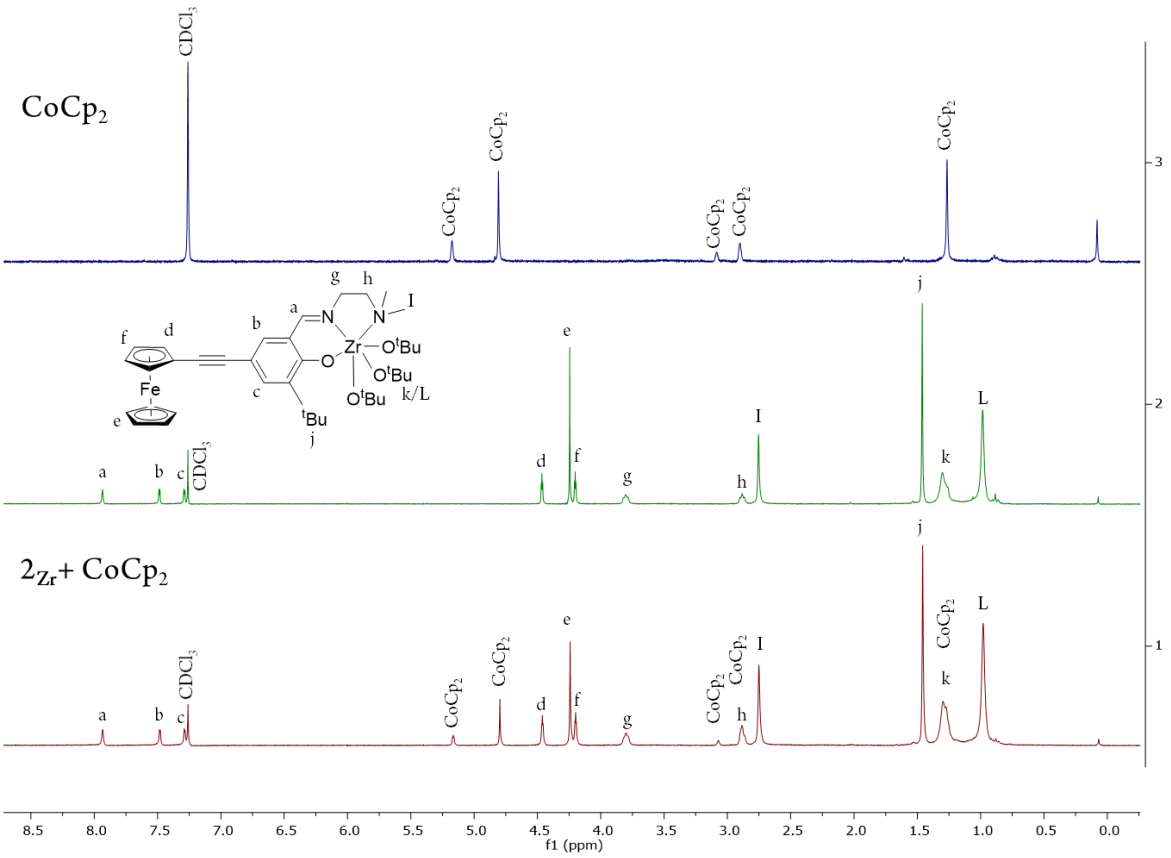

Figure S17. ^{1}H NMR spectra (300 MHz, 25 °C, $CDCl_3$) of $\mathbf{2_{Zr}}$ + 1.2 eq. $CoCp_2$ (bottom), $\mathbf{2_{Zr}}$ (middle), and $CoCp_2$ (top). Every peak in the bottom spectrum can be accounted for from either the middle or top spectra indicating that the $CoCp_2$ has no direct effect on $\mathbf{2_{Zr}}$.

Polymerization Data

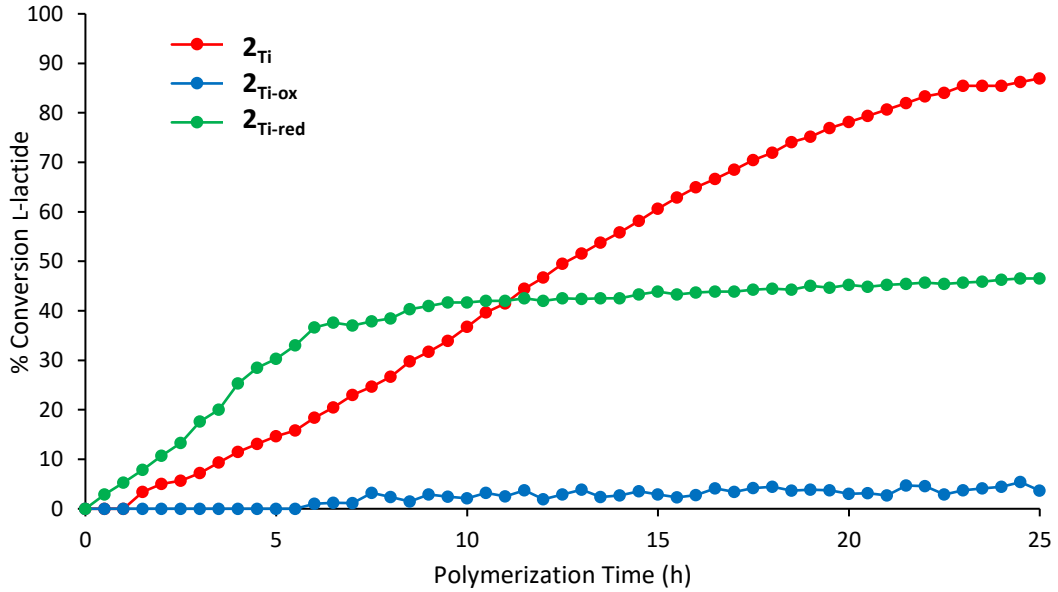

Figure S18. Plot of monomer conversion (%) versus time (h) for the polymerization of L-lactide (100 eq, 1M) in $CDCl_3$ at 90 °C using $\mathbf{2}_{Ti}$ (red circles), $\mathbf{2}_{Ti\text{-}ox}$ (blue circles), and $\mathbf{2}_{Ti\text{-}red}$ (green circles). Using $AgBAr^F$ as an oxidizing agent and $CoCp_2$ as a reducing agent.

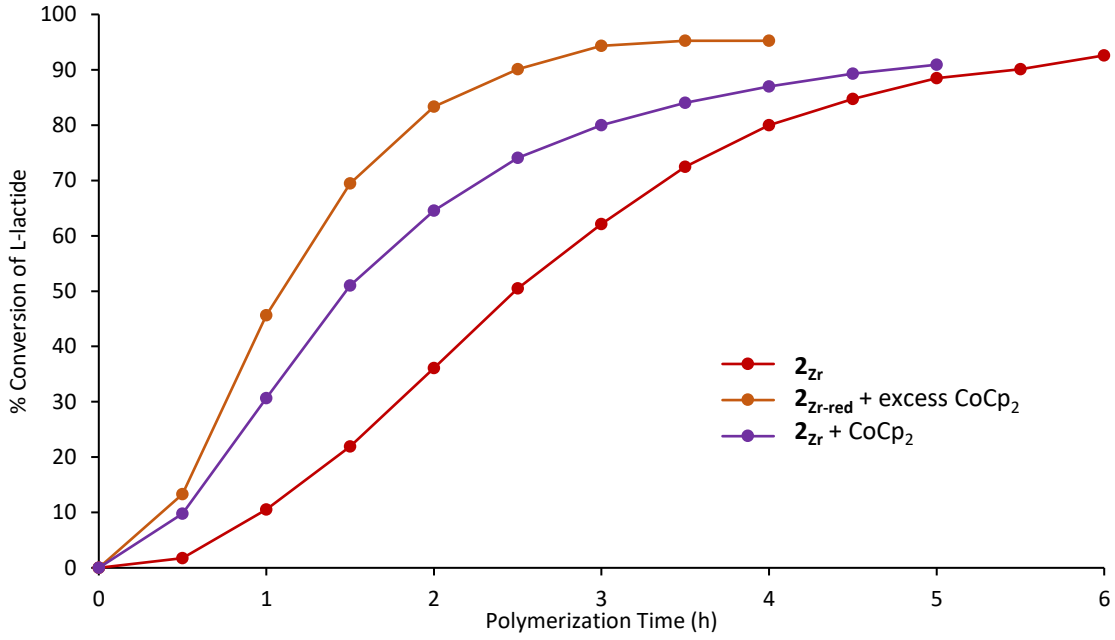

Figure S19. Plot of monomer conversion (%) versus time (h) for the polymerization of L-lactide (100 eq, 1 M) in $CDCl_3$ at 90 °C using $\mathbf{2}_{Zr}$ (red circles), $\mathbf{2}_{Zr}$ + 1 eq. $CoCp_2$ (purple circles), and $\mathbf{2}_{Zr\text{-}red}$ generated with excess (1.5 eq.) $CoCp_2$ (orange circles).

Cyclic Voltammetry

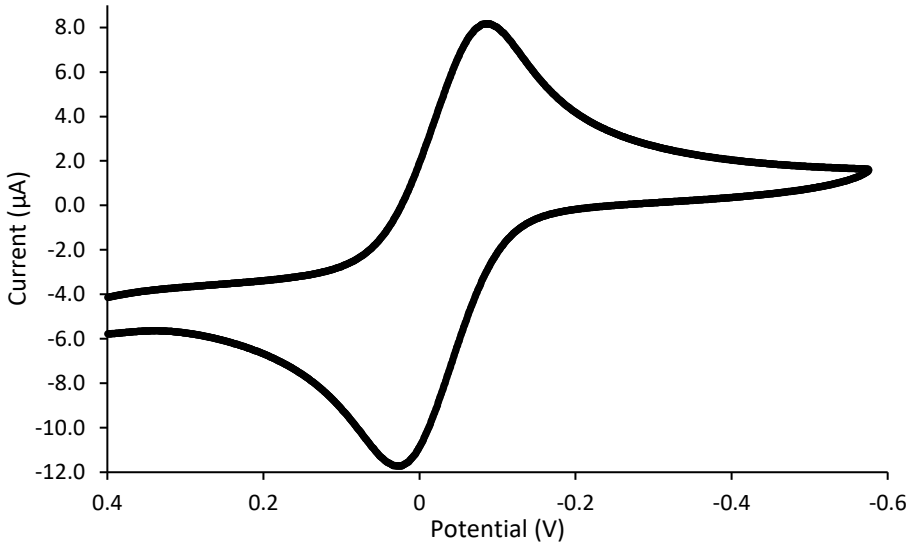

Figure S20. Cyclic voltammogram of catalyst $\mathbf{2_{Ti}}$ (0.01 mmol) recorded at a scan rate of 100 mV/s in dichloromethane (5 mL), $(n\text{Bu})_4\text{NPF}_6$ (0.20 M), ($E_{1/2}$ = -0.03 V) versus Fc/Fc^+.

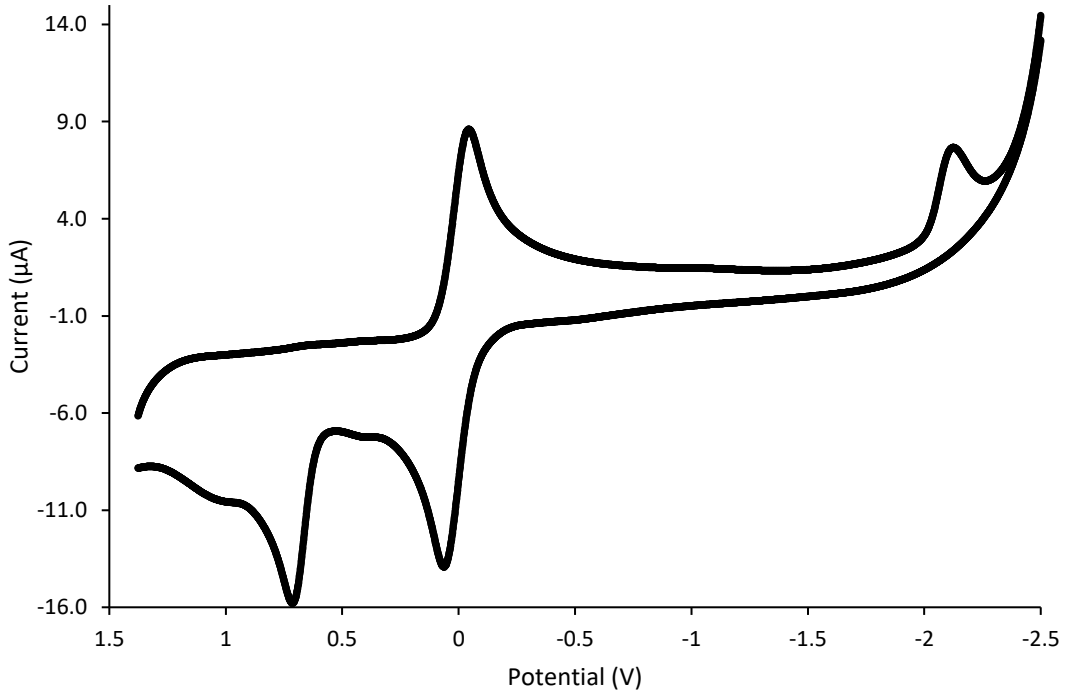

Figure S21. Cyclic voltammogram of catalyst $\mathbf{2_{Zr}}$ (0.01 mmol) recorded at a scan rate of 100 mV/s in dichloromethane (5 mL), $(n\text{Bu})_4\text{NPF}_6$ (0.20 M), ($E_{1/2}$ = 0.03 V) versus Fc/Fc^+.

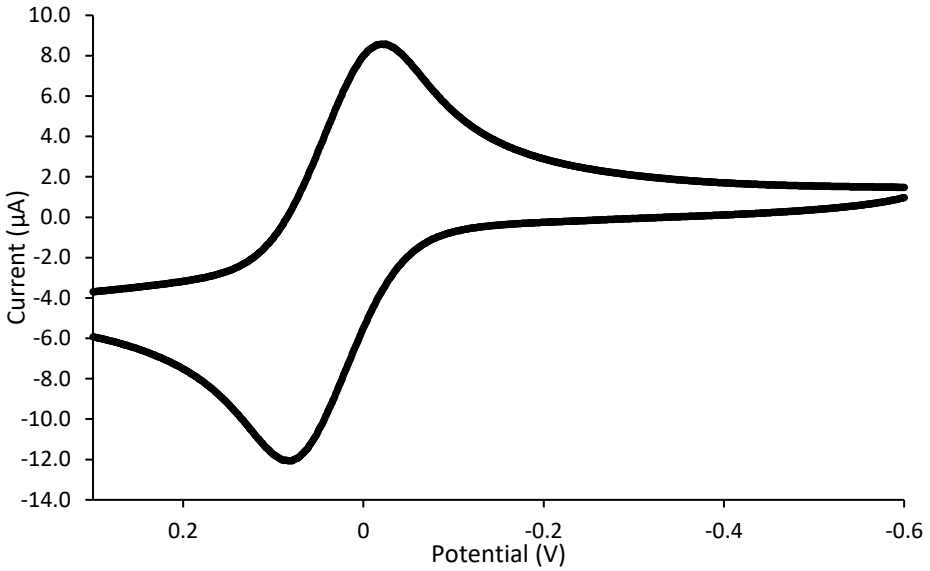

Figure S22. Zoomed in cyclic voltammogram of catalyst $\mathbf{2_{Zr}}$ (0.01 mmol) recorded at a scan rate of 100 mV/s in dichloromethane (5 mL), $(n\text{Bu})_4\text{NPF}_6$ (0.20 M), ($E_{1/2}$ = 0.03 V) versus Fc/Fc^+.

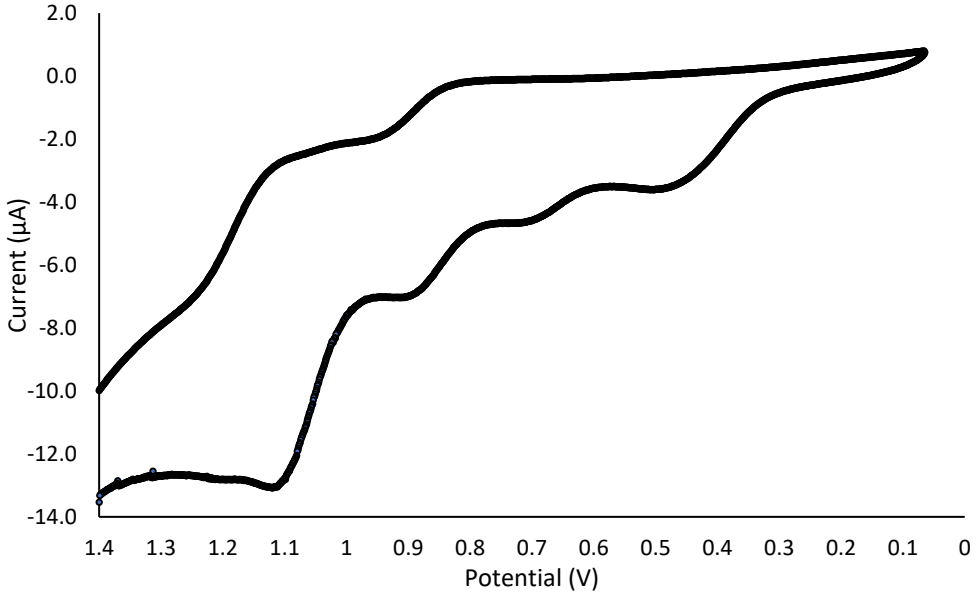

Figure S23. Cyclic voltammogram of catalyst $\mathbf{3_{Ti}}$ (0.01 mmol) recorded at a scan rate of 100 mV/s in dichloromethane (5 mL), $(n\text{Bu})_4\text{NPF}_6$ (0.20 M).

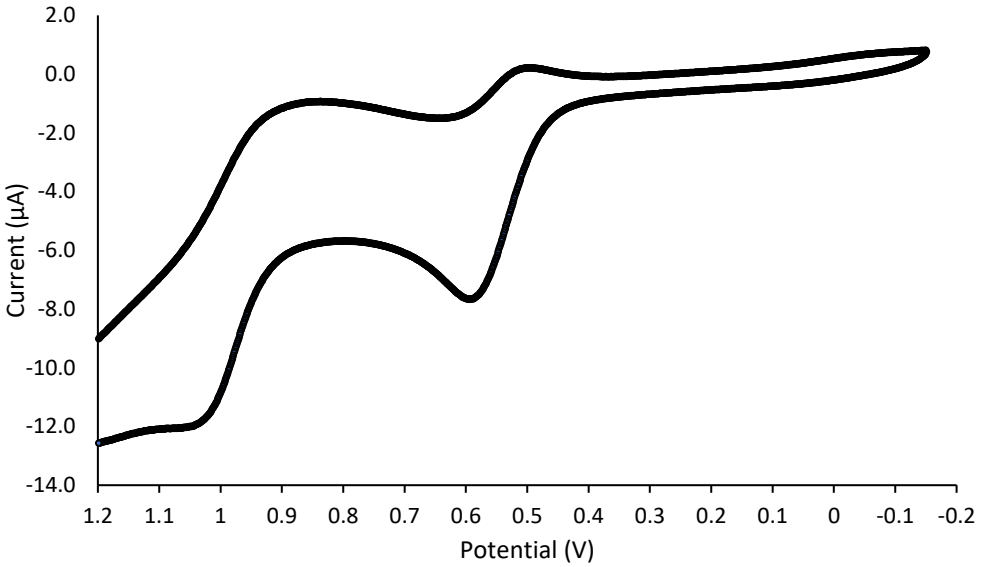

Figure S24. Cyclic voltammogram of catalyst $\mathbf{3_{Zr}}$ (0.01 mmol) recorded at a scan rate of 100 mV/s in dichloromethane (5 mL), $(n\text{Bu})_4\text{NPF}_6$ (0.20 M).

UV-Vis Spectra

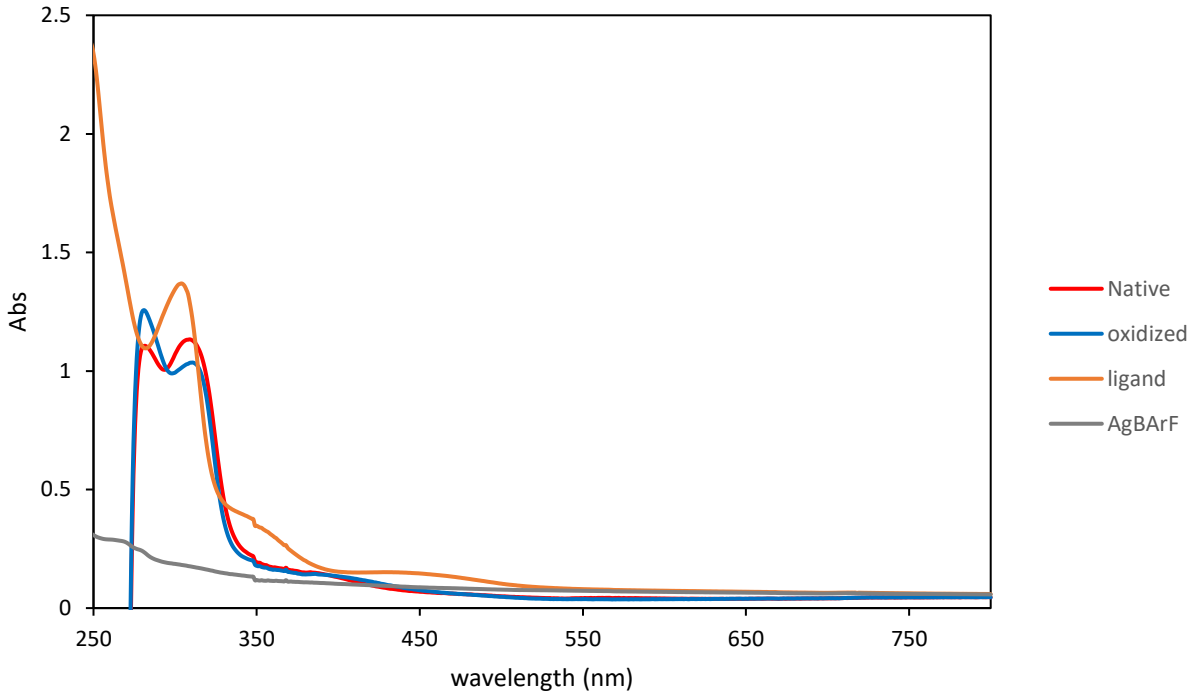

Figure S25. UV-Vis Spectra of $\mathbf{2}_{Zr}$ (4.2 x 10^{-5} M) (red), $\mathbf{2}_{Zr\text{-}ox}$ (4.2 x 10^{-5} M) (blue), **L2** (4.2 x 10^{-5} M) (orange), and $AgBAr^{F}$ (4.2 x 10^{-5} M) (gray).

X-Ray Crystallographic Data

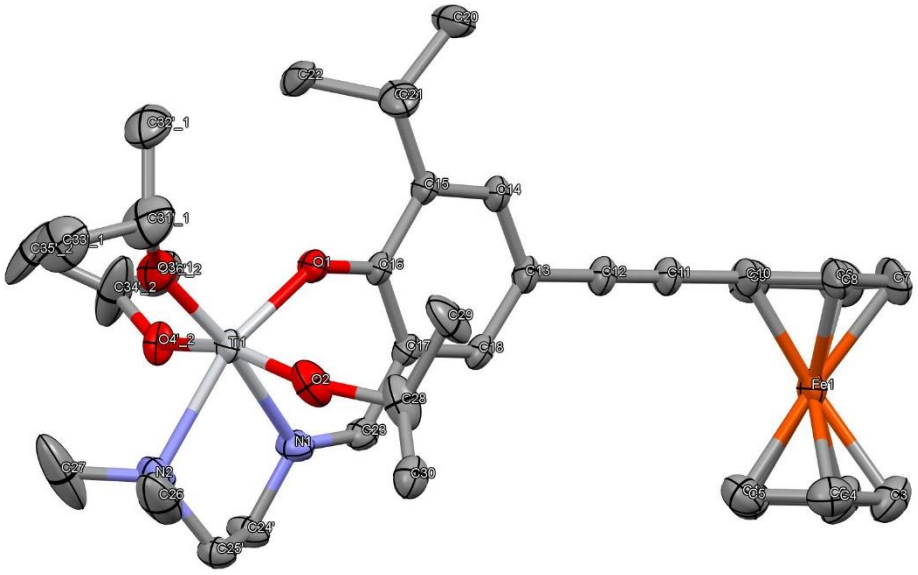

Figure S26. ShelXle representation of $\mathbf{2_{Ti}}$ with thermal ellipsoids drawn at 50% probability. Hydrogens were omitted for clarity. X-ray quality single crystals of $\mathbf{2_{Ti}}$ were obtained via recrystallization from hexanes upon cooling to -20 °C. Crystal data for $C_{36}H_{55}FeN_2O_4Ti$ (680.53 g/mol); monoclinic; space group P2(1)/c; *a*= 22.6283(13) Å; *b*= 8.7736(5) Å; *c*= 18.5643(10) Å; α= 90°; β= 105.170(2)°; γ = 90°; V = 3557.2(3) $Å^3$; Z = 2; T = 100(2) K; λ= 0.71073 Å; μ= 0.670 mm^{-1}; R_1= 0.0496; wR_2= 0.1381 for 44,451 reflections; GOF = 1.027. CCDC Reference Number: 1993768

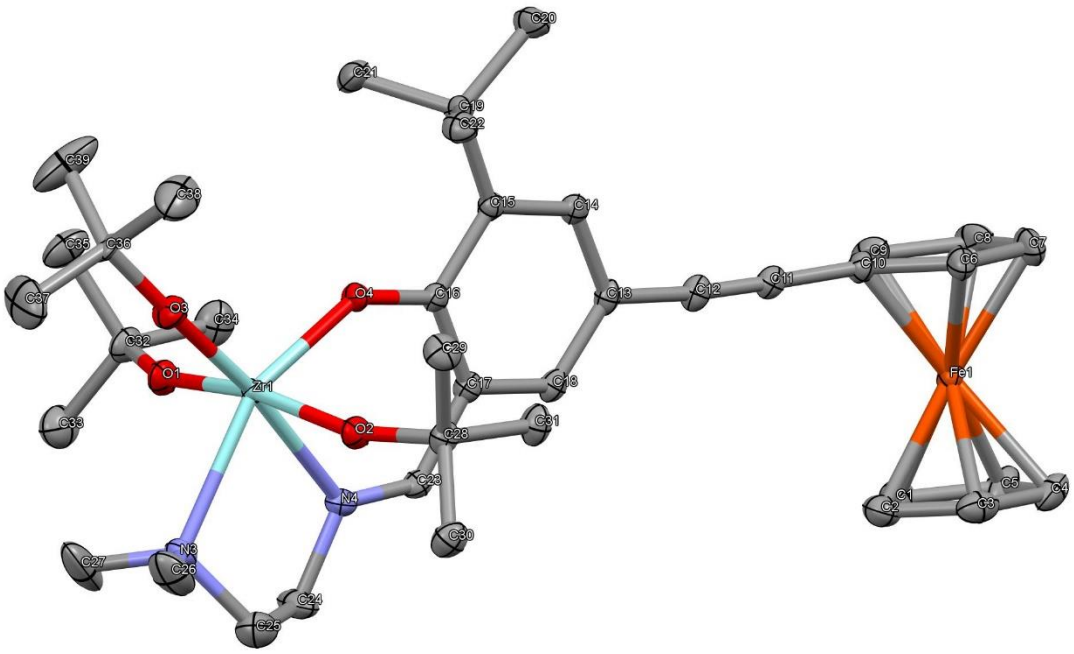

Figure S27. ShelXle representation of $\mathbf{2_{Zr}}$ with thermal ellipsoids drawn at 50% probability. Hydrogens were omitted for clarity. X-ray quality single crystals of $\mathbf{2_{Zr}}$ were obtained via recrystallization from hexanes upon cooling to -20 °C. Crystal data for $C_{39}H_{58}FeN_2O_4Zr$ (765.97 g/mol); monoclinic; space group P2(1)/c; *a*= 22.8642(12) Å; *b*= 9.1582(5) Å; *c*= 19.4463(10) Å; α= 90°; β= 106.4470(10)°; γ = 90°; V = 3905.3(4) $Å^3$; Z = 4; T = 100(2) K; λ= 0.71073 Å; μ= 0.677 mm^{-1}; R_1= 0.0353; wR_2= 0.0841 for 51,591 reflections; GOF = 1.011. CCDC Reference Number: 1993769

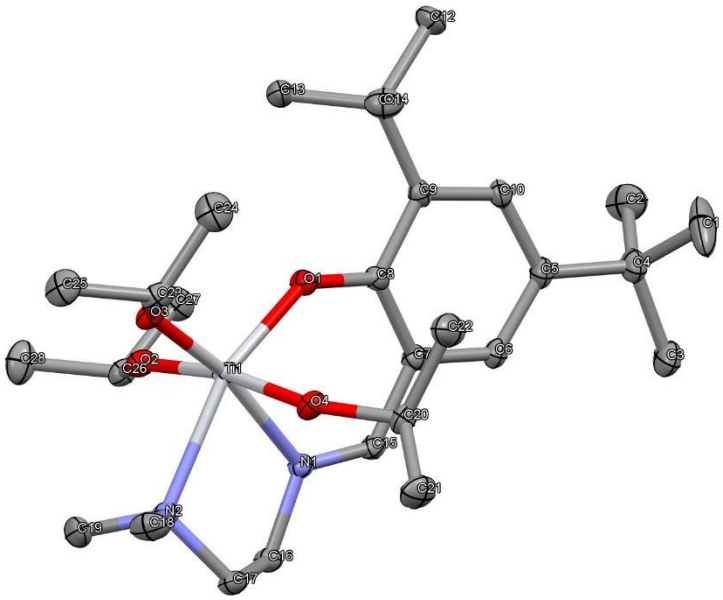

Figure S28. ShelXle representation of $\mathbf{3_{Ti}}$ with thermal ellipsoids drawn at 50% probability. Hydrogens and pentane molecules were omitted for clarity. X-ray quality single crystals of $\mathbf{3_{Ti}}$ were obtained via recrystallization from a concentrated pentanes solution upon cooling to -20 °C. Crystal data for $C_{28}H_{52}N_2O_4Ti$ (528.60 g/mol); monoclinic; space group P2(1)/c; *a*= 26.1034(16) Å; *b*= 13.6068(8) Å; *c*= 18.7389(11) Å; α= 90°; β= 90.427(2)°; γ = 90°; V = 6655.6(7) $Å^3$; Z = 14; T = 100(2) K; λ= 0.71073 Å; μ= 0.290 mm^{-1}; R_1= 0.0656; wR_2= 0.1482 for 202,143 reflections; GOF = 1.185. CCDC Reference Number: 1993770

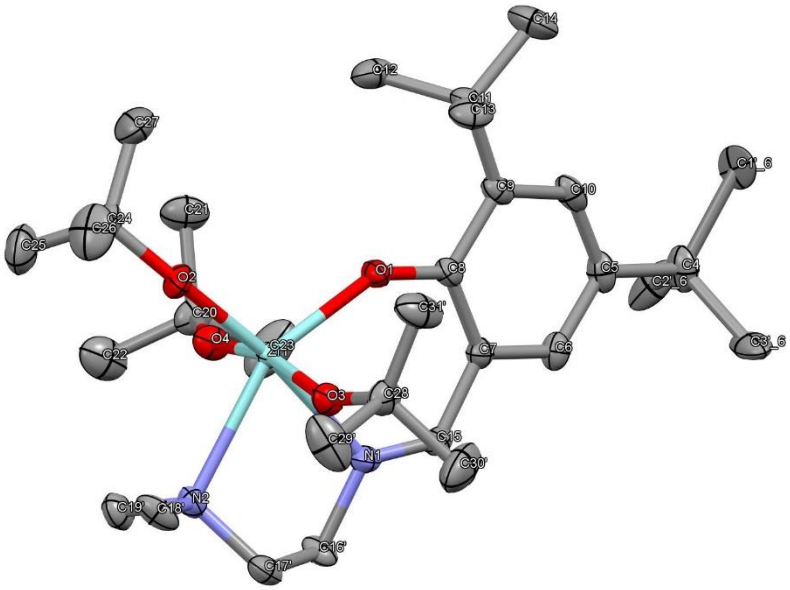

Figure S29. ShelXle representation of $\mathbf{3_{Zr}}$ with thermal ellipsoids drawn at 50% probability. Hydrogens were omitted for clarity. X-ray quality single crystals of $\mathbf{3_{Zr}}$ were obtained via recrystallization from a concentrated pentanes solution upon cooling to -20 °C. Crystal data for $C_{31}H_{58}N_2O_4Zr$ (614.04 g/mol); triclinic; space group P-1; *a*= 9.0808(8) Å; *b*= 9.9464(8) Å; *c*= 21.5037(18) Å; α= 93.147(3)°; β= 91.175(3)°; γ = 115.995(2)°; V = 1741.0(3) $Å^3$; Z = 2; T = 100(2) K; λ= 0.71073 Å; μ= 0.349 mm^{-1}; R_1= 0.0459; wR_2= 0.1051 for 60,166 reflections; GOF = 0.918. CCDC Reference Number: 1993771

GPC Analysis of Polymers

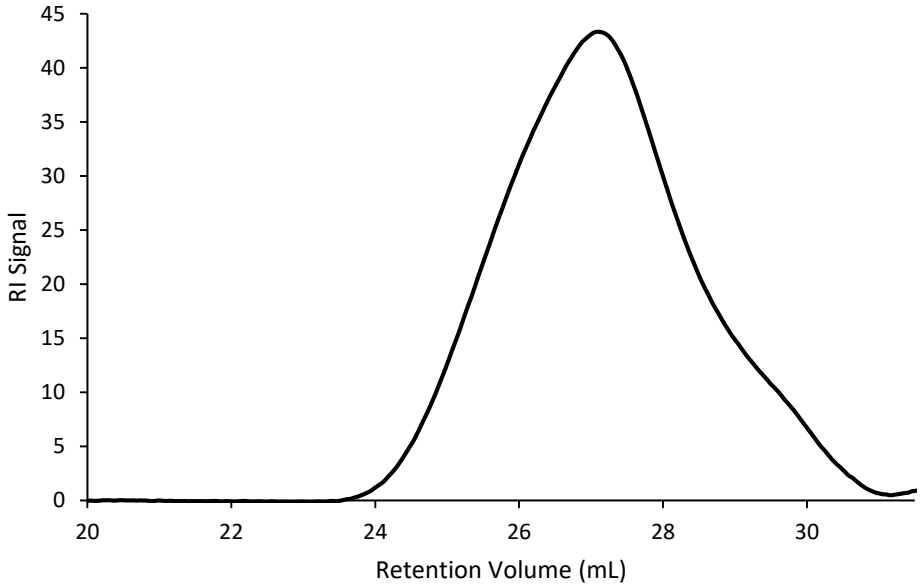

Figure S30. GPC trace of PLA obtained using $\mathbf{2_{Ti}}$. Samples measured in THF at 30 °C and reported as absolute molecular weights (Table 1, Entry 1).

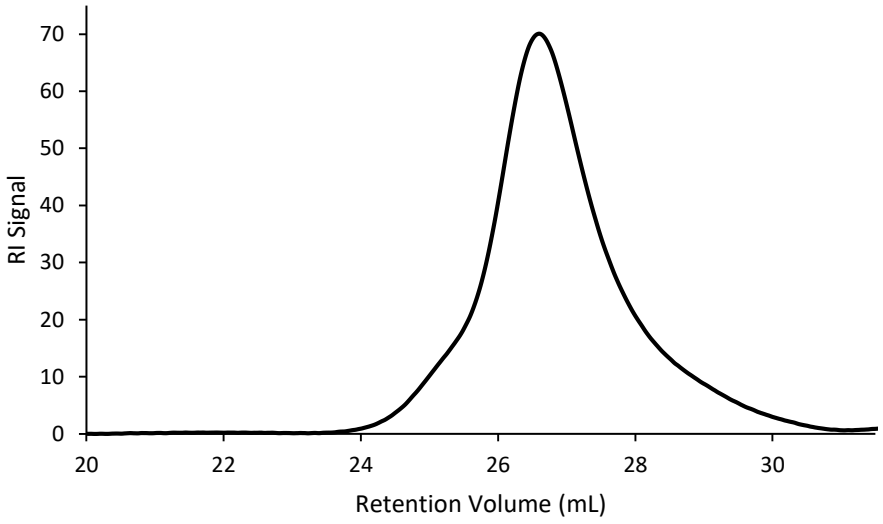

Figure S31. GPC trace of PLA obtained using $\mathbf{2_{Zr}}$. Samples measured in THF at 30 °C and reported as absolute molecular weights (Table 1, Entry 2).

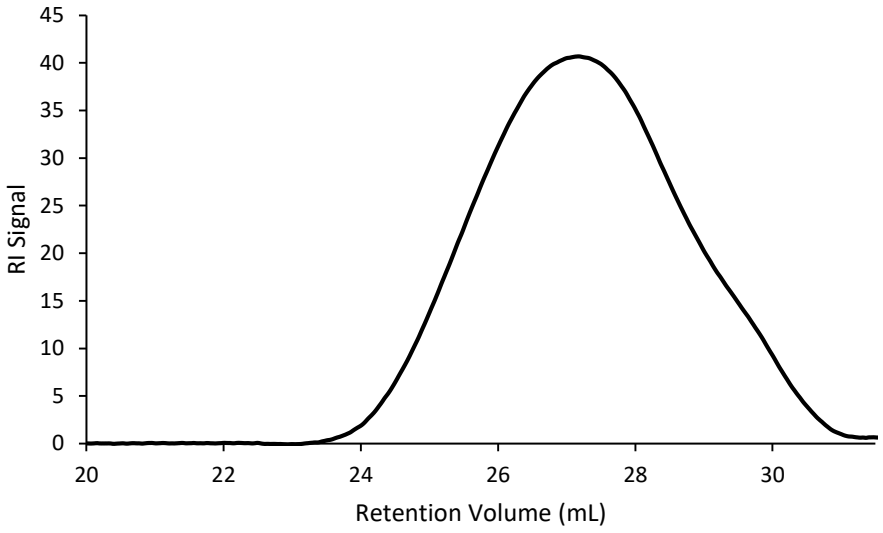

Figure S32. GPC trace of PLA obtained using $\mathbf{3_{Ti}}$. Samples measured in THF at 30 °C and reported as absolute molecular weights (Table 1, Entry 3).

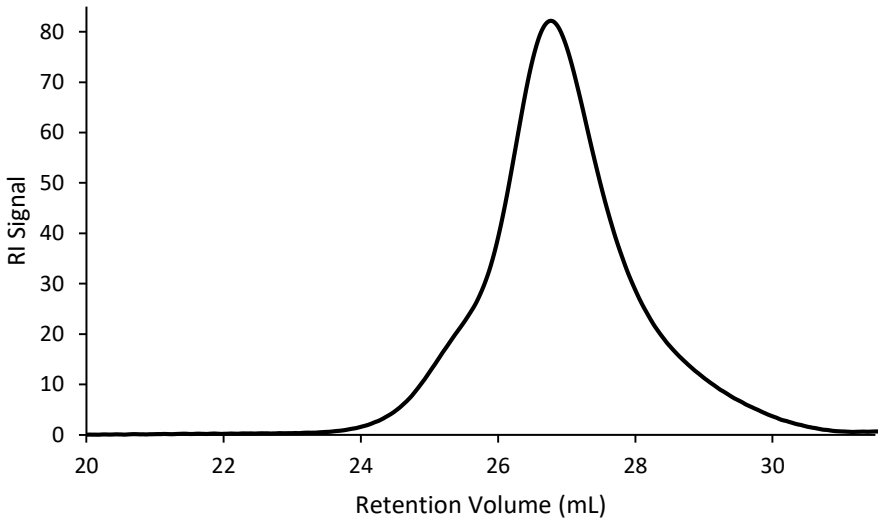

Figure S33. GPC trace of PLA obtained using $\mathbf{3_{Zr}}$. Samples measured in THF at 30 ° C and reported as absolute molecular weights (Table 1, Entry 4).

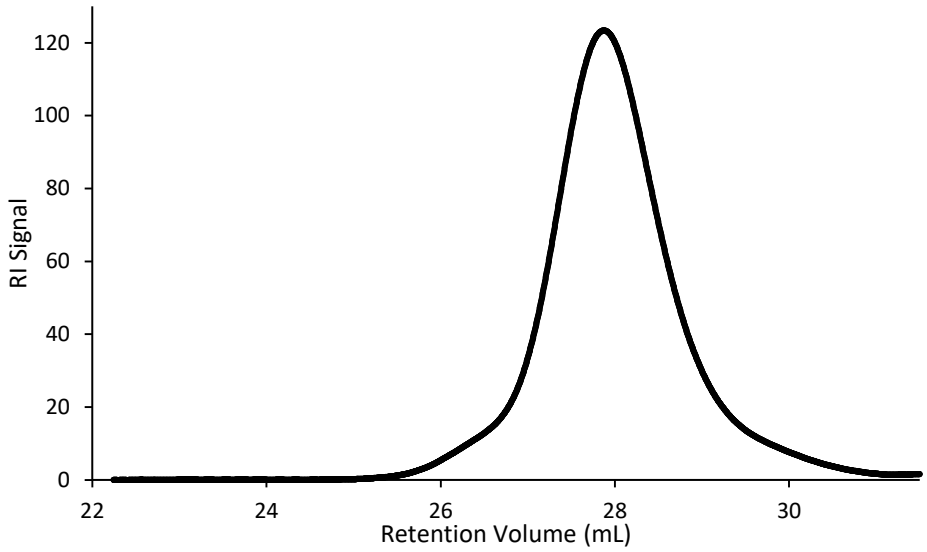

Figure S34. GPC trace of PLA obtained using $\mathbf{2}_{\mathbf{Zr}}$. Samples measured in THF at 30 ° C and reported as absolute molecular weights.

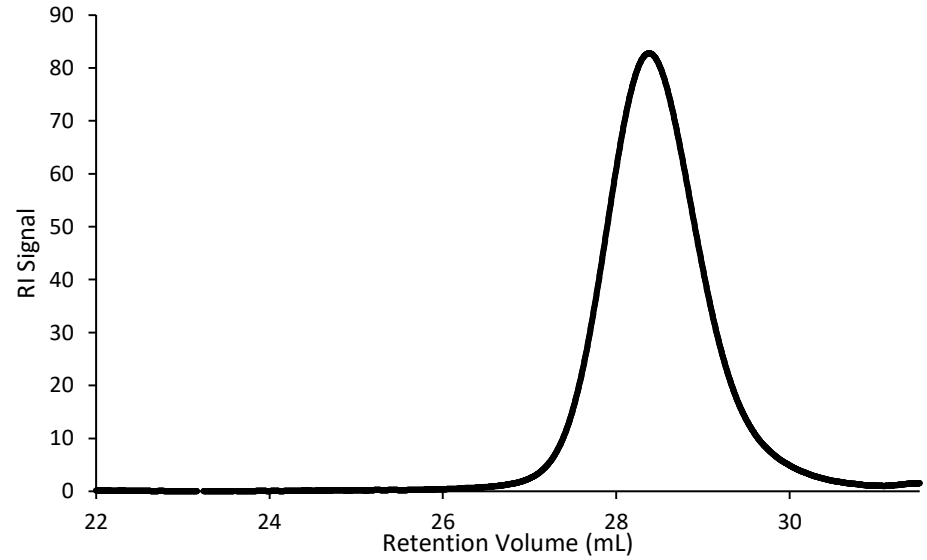

Figure S35. GPC trace of PLA obtained using $\mathbf{2}_{\mathbf{Zr\text{-}red}}$. Samples measured in THF at 30 ° C and reported as absolute molecular weights.

Kinetic Study for L-Lactide Polymerization

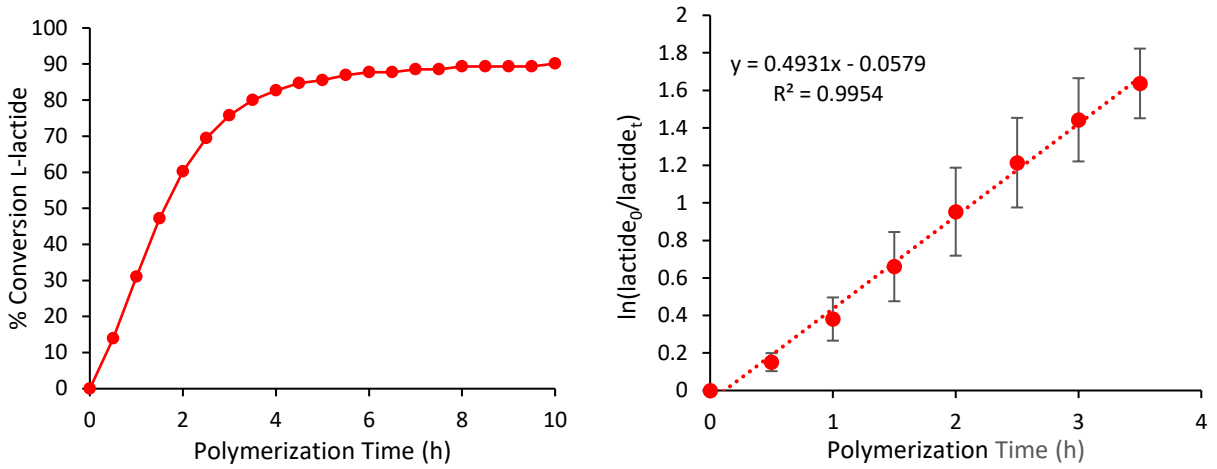

Figure S36. Polymerization of 100 equivalents of L-lactide in C_6D_6 at 90 °C using **1** (left graph), and a plot of ln(L-lactide$_0$/L-lactide$_t$) vs time (h) to study the polymerization kinetics (right graph).

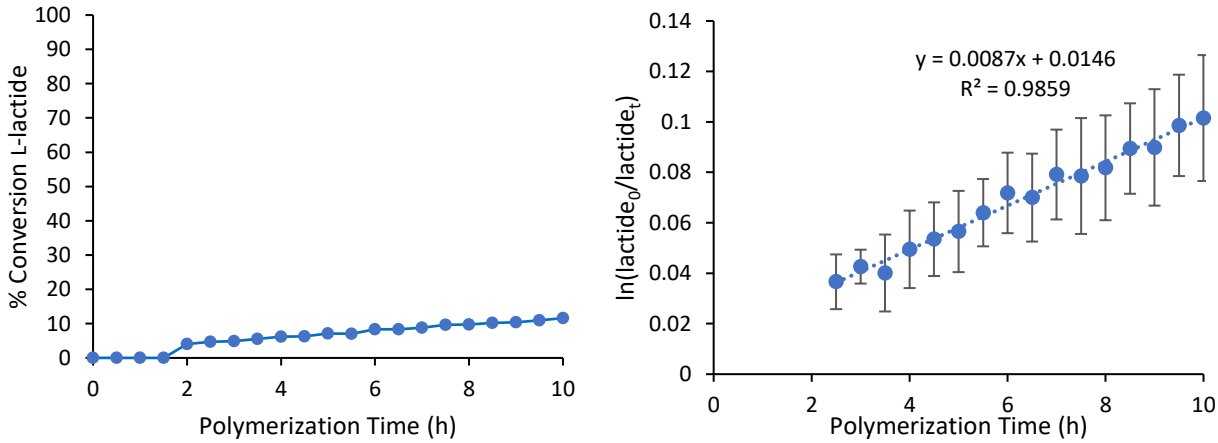

Figure S37. Polymerization of 100 equivalents of L-lactide in C_6D_6 at 90 °C using $\mathbf{1_{ox}}$ (left graph), and a plot of ln(L-lactide$_0$/L-lactide$_t$) vs time (h) to study the polymerization kinetics (right graph).

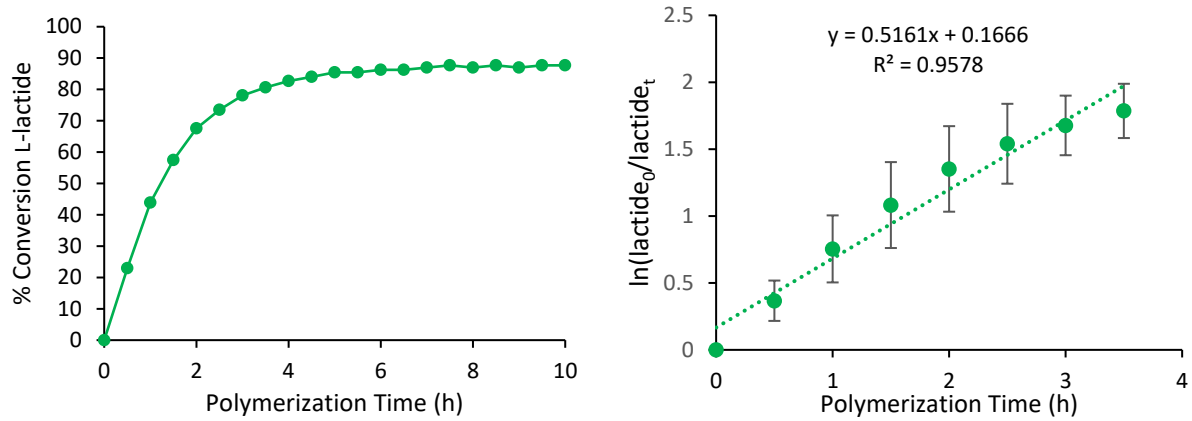

Figure S38. Polymerization of 100 equivalents of L-lactide in C_6D_6 at 90 °C using $\mathbf{1}_{red}$ (left graph), and a plot of ln(L-lactide$_0$/L-lactide$_t$) vs time (h) to study the polymerization kinetics (right graph).

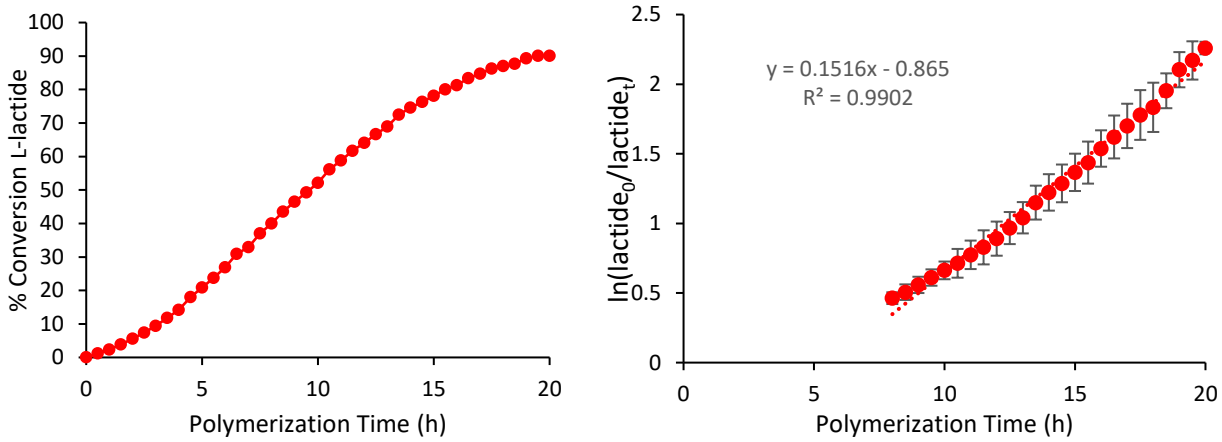

Figure S39. Polymerization of 100 equivalents of L-lactide in C_6D_6 at 90 °C using $\mathbf{2}_{Ti}$ (left graph), and a plot of ln(L-lactide$_0$/L-lactide$_t$) vs time (h) to study the polymerization kinetics (right graph).

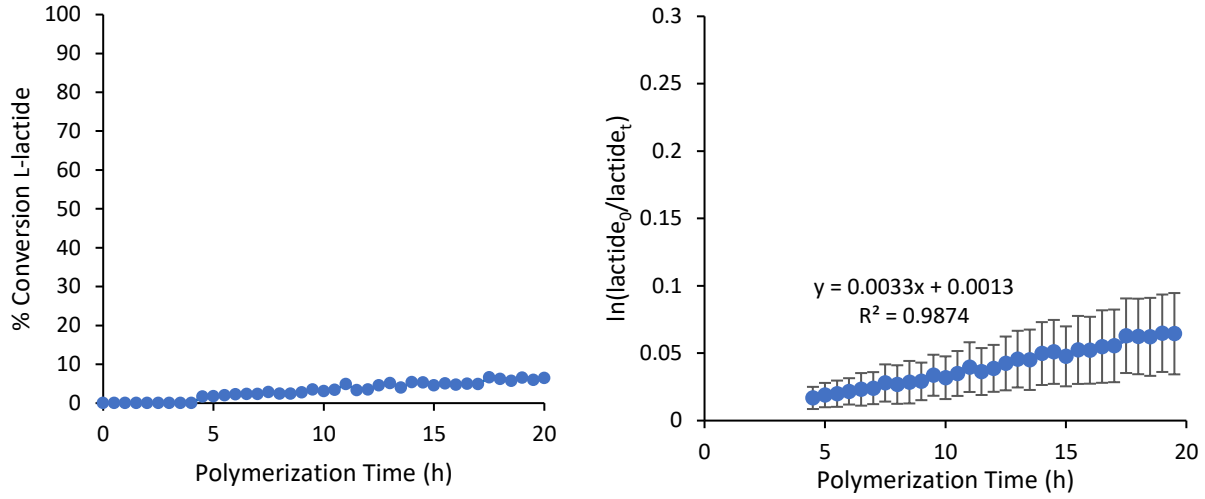

Figure S40. Polymerization of 100 equivalents of L-lactide in C_6D_6 at 90 °C using $\mathbf{2}_{\mathbf{Ti\text{-}ox}}$ (left graph), and a plot of ln(L-lactide$_0$/L-lactide$_t$) vs time (h) to study the polymerization kinetics (right graph).

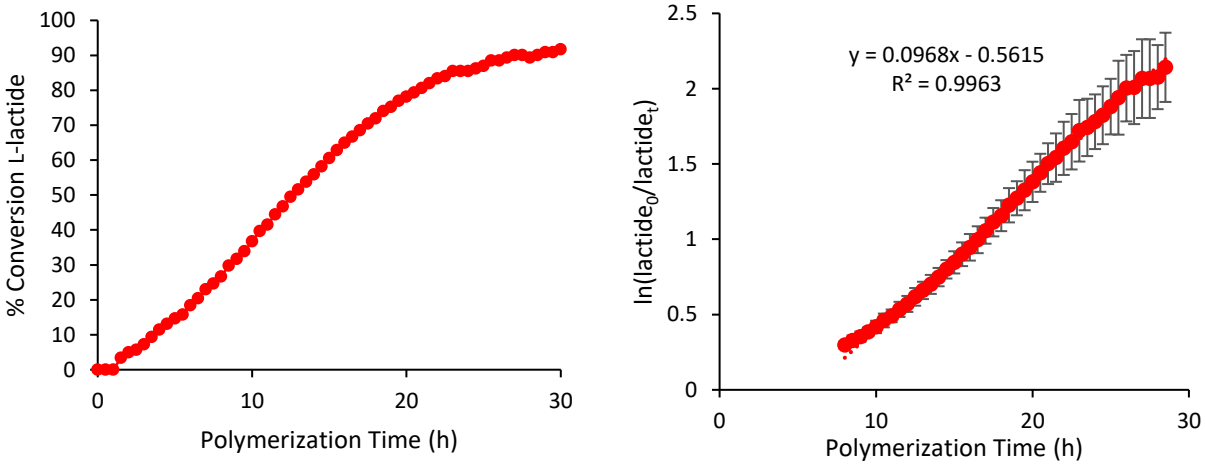

Figure S41. Polymerization of 100 equivalents of L-lactide in $CDCl_3$ at 90 °C using $\mathbf{2}_{\mathbf{Ti}}$ (left graph), and a plot of ln(L-lactide$_0$/L-lactide$_t$) vs time (h) to study the polymerization kinetics (right graph).

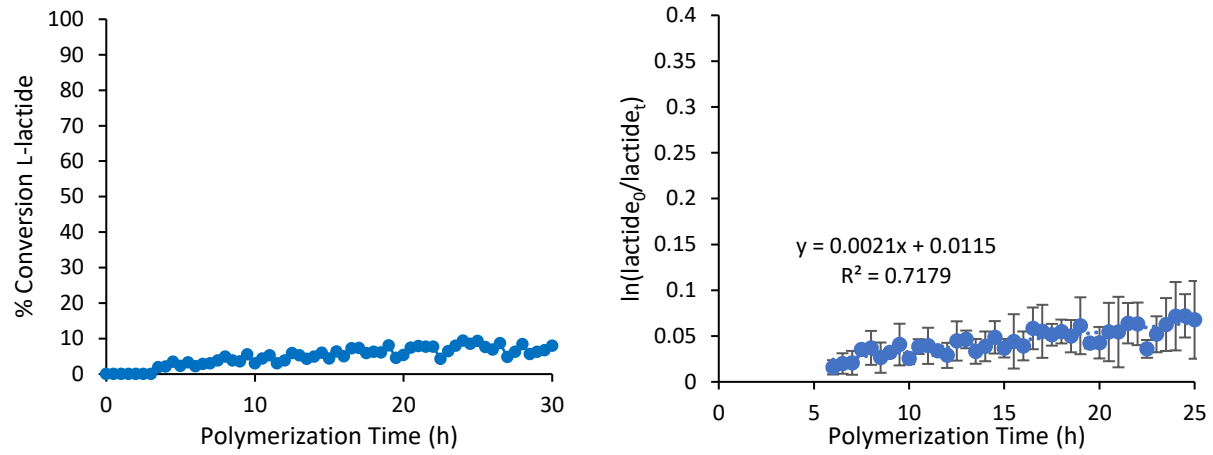

Figure S42. Polymerization of 100 equivalents of L-lactide in $CDCl_3$ at 90 °C using $\mathbf{2_{Ti\text{-}ox}}$ (left graph), and a plot of ln(L-lactide$_0$/L-lactide$_t$) vs time (h) to study the polymerization kinetics (right graph).

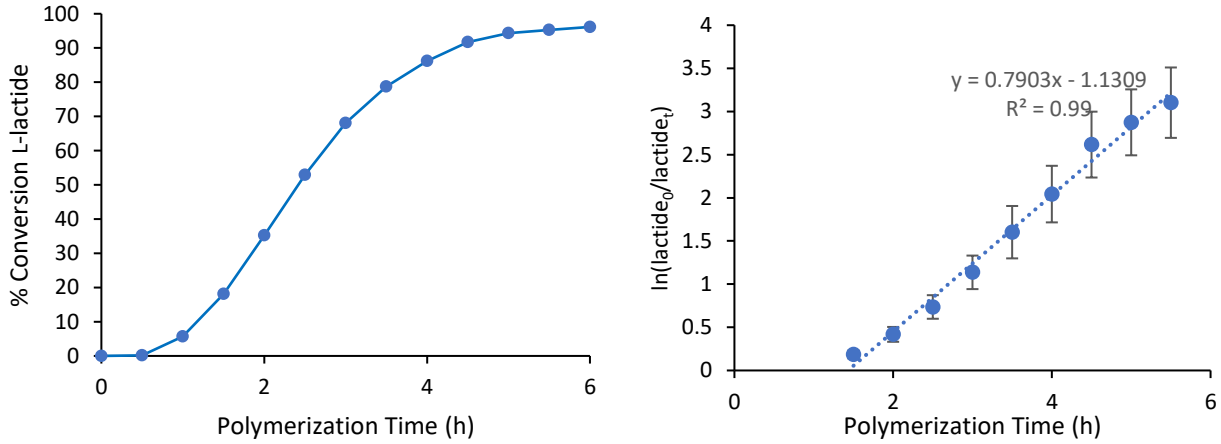

Figure S43. Polymerization of 100 equivalents of L-lactide in C_6D_6 at 90 °C using $\mathbf{2_{Zr}}$ (left graph), and a plot of ln(L-lactide$_0$/L-lactide$_t$) vs time (h) to study the polymerization kinetics (right graph).

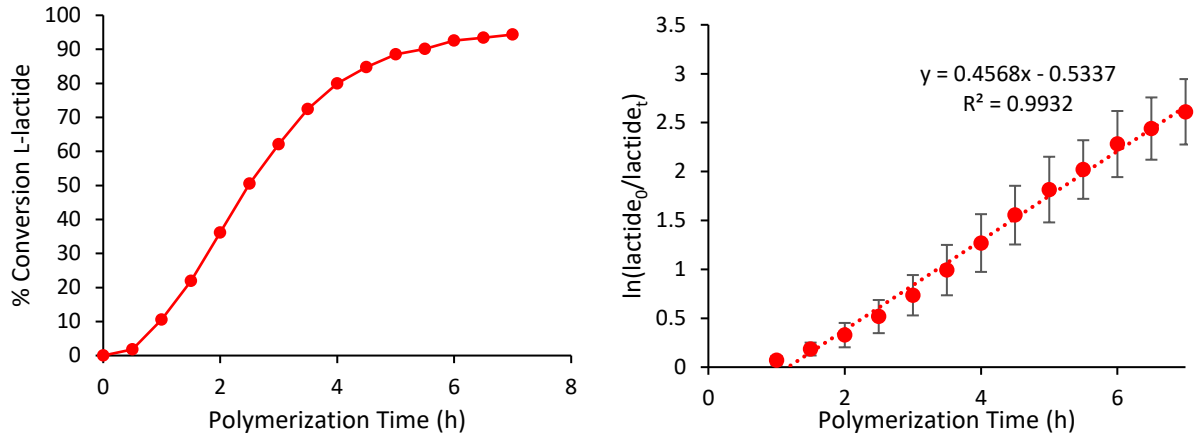

Figure S44. Polymerization of 100 equivalents of L-lactide in $CDCl_3$ at 90 °C using $\mathbf{2_{Zr}}$ (left graph), and a plot of ln(L-lactide$_0$/L-lactide$_t$) vs time (h) to study the polymerization kinetics (right graph).

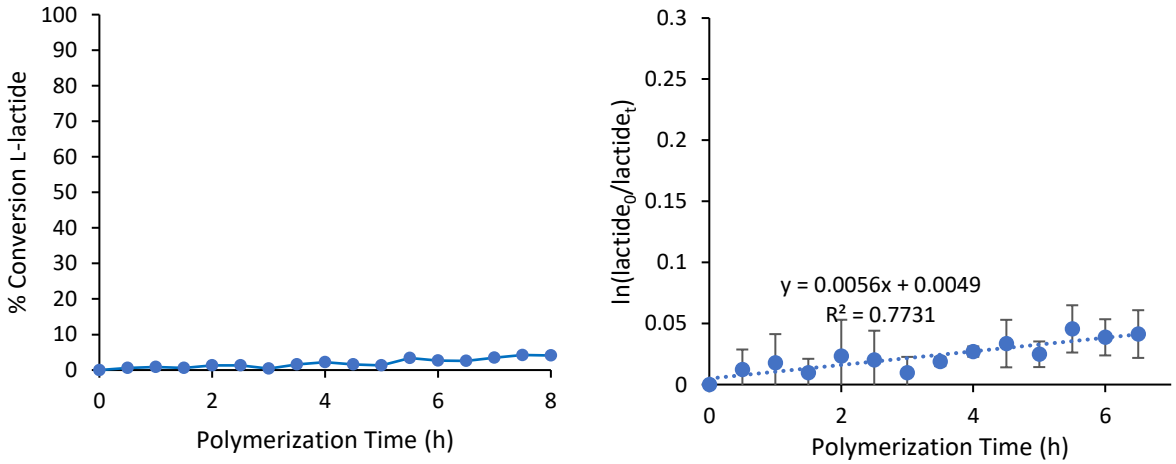

Figure S45. Polymerization of 100 equivalents of L-lactide in $CDCl_3$ at 90 °C using $\mathbf{2_{Zr\text{-}ox}}$ (left graph), and a plot of ln(L-lactide$_0$/L-lactide$_t$) vs time (h) to study the polymerization kinetics (right graph).

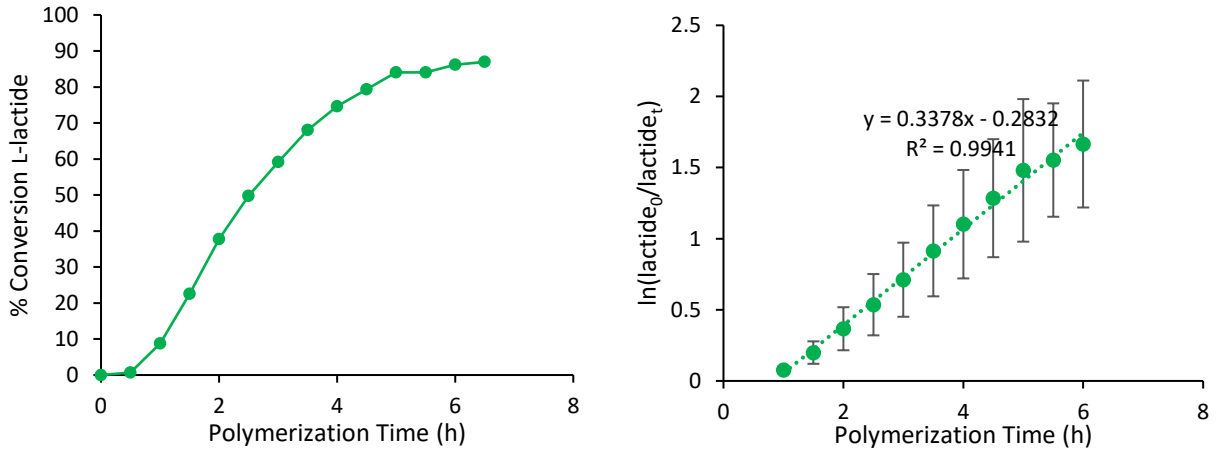

Figure S46. Polymerization of 100 equivalents of L-lactide in $CDCl_3$ at 90 °C using $\mathbf{2}_{\mathbf{Zr\text{-}red}}$ (left graph), and a plot of ln(L-lactide$_0$/L-lactide$_t$) vs time (h) to study the polymerization kinetics (right graph).

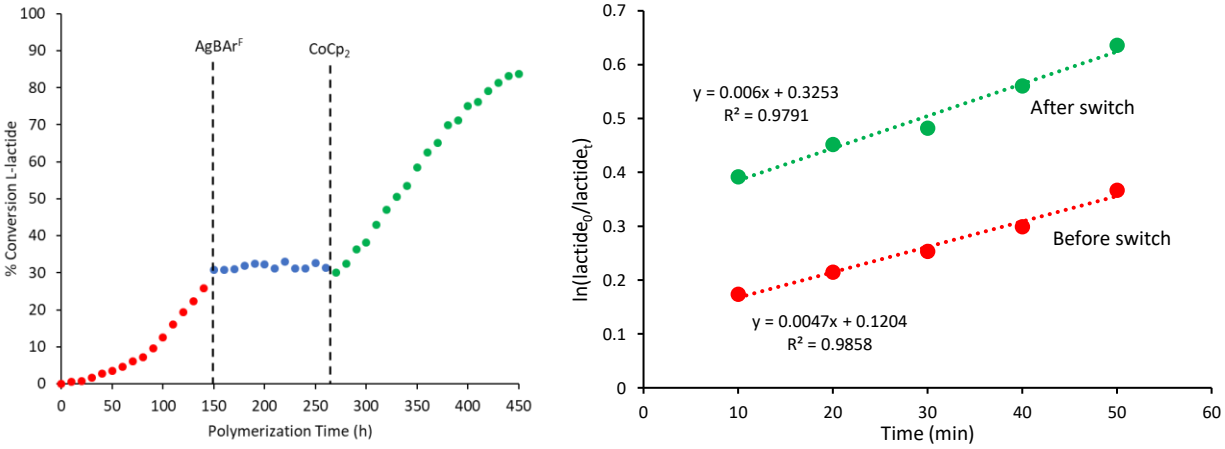

Figure S47. *In situ* switching polymerization of 100 equivalents of L-lactide in $CDCl_3$ at 90 °C starting from native catalyst $\mathbf{2}_{\mathbf{Zr}}$ and switching at 2.5 hours and 4.5 hours (left graph), and a plot of ln(L-lactide$_0$/L-lactide$_t$) vs time (min) to study the polymerization kinetics before and after the switch (right graph).

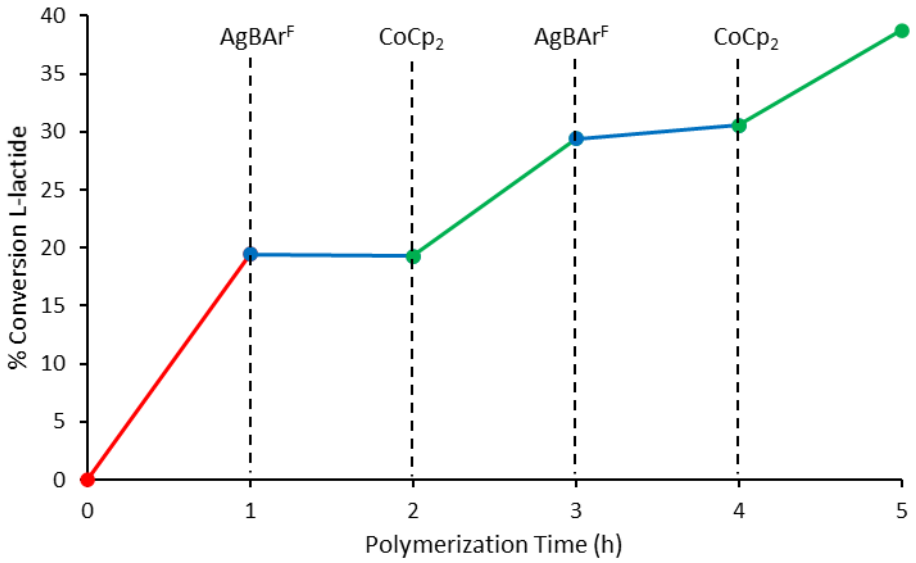

Figure S48. *In situ* switching polymerization of 100 equivalents of L-lactide in $CDCl_3$ at 90 °C starting from native catalyst $\mathbf{2}_{Zr}$ and switching to $\mathbf{2}_{Zr\text{-}ox}$ with the addition of 1 eq. AgBAr^F and $\mathbf{2}_{Zr\text{-}red}$ with the addition of 1 eq. $CoCp_2$ at the indicated time points.

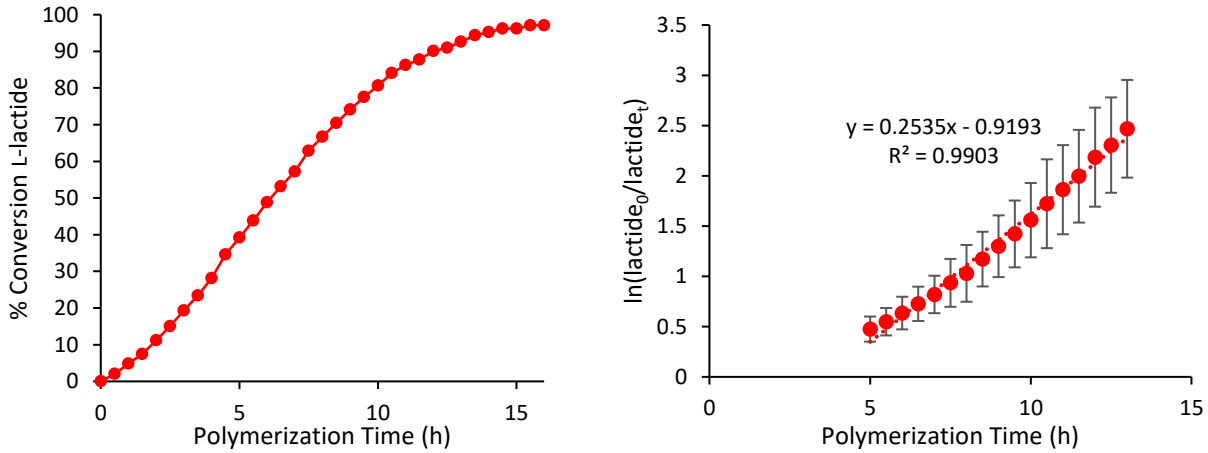

Figure S49. Polymerization of 100 equivalents of L-lactide in C_6D_6 at 90 °C using $\mathbf{3}_{Ti}$ (left graph), and a plot of ln(L-lactide$_0$/L-lactide$_t$) vs time (h) to study the polymerization kinetics (right graph).

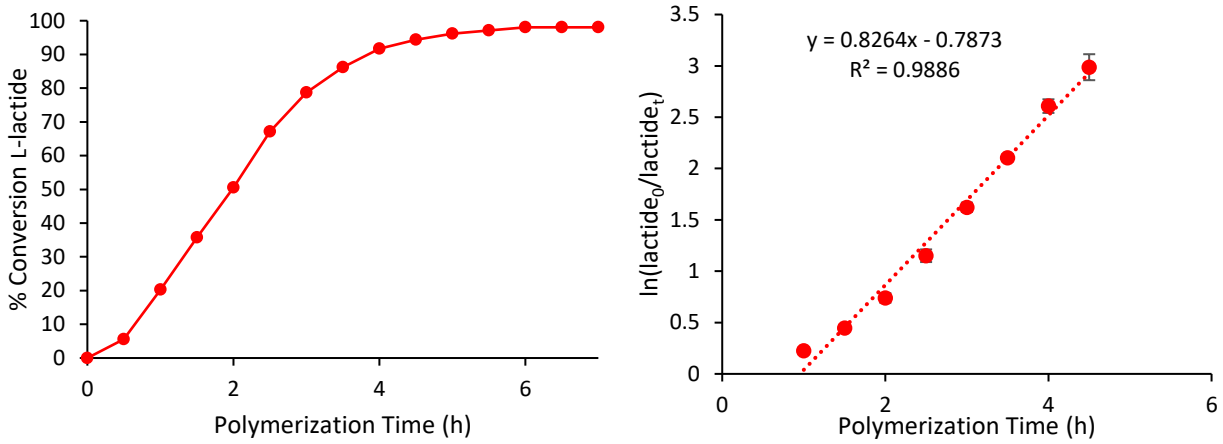

Figure S50. Polymerization of 100 equivalents of L-lactide in C_6D_6 at 90 °C using $\mathbf{3_{Zr}}$ (left graph), and a plot of ln(L-lactide$_0$/L-lactide$_t$) vs time (h) to study the polymerization kinetics (right graph).

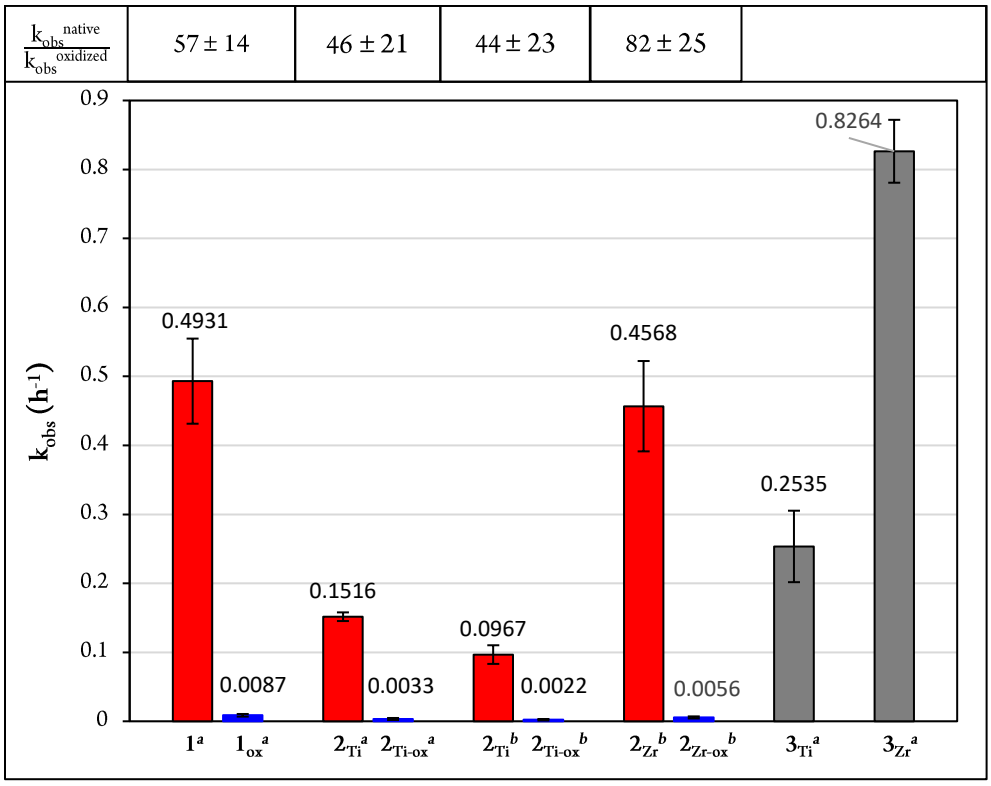

Figure S51. Comparison of k_{obs} for each catalyst in the native state and oxidized state (when applicable). Conditions: 10 µmol catalyst, 0.7 mmol L-lactide, 1 M, 90 °C. [a]solvent = C_6D_6, [b]solvent = $CDCl_3$.